Postgraduate Program in Environmental Physics (PEP)

Institute of Environmental Physics (IUP)

University of Bremen

Master Thesis

Validation of GEMS satellite observations of NO_2 using Ground-based DOAS-measurements in Seoul

Author: Chisom Maurice Okafor

First Examiner: Dr. Andreas Richter

Second Examiner: PD Dr. Warneke, Thorsten

Acknowledgement

I would like to express my deepest gratitude to my supervisor, Dr. Andreas Richter, for his invaluable guidance, encouragement, and expertise throughout the course of this research. His insights and constructive criticism were instrumental in shaping both the direction and success of this thesis. Dr. Richter's unwavering support and commitment to academic excellence have been a constant source of inspiration and motivation for me.

I am also profoundly thankful to PD Dr. Thorsten Warneke, my second examiner, for his critical evaluations and insightful feedback. His thorough reviews and suggestions have significantly contributed to the refinement and quality of this work. I deeply appreciate his time and efforts in carefully examining my thesis.

The journey of completing this thesis was not only an academic challenge but also a period of personal growth, and I am grateful for having had the guidance of such distinguished and dedicated academics. Their knowledge and dedication to the field of atmospheric sciences have left an indelible mark on my professional development.

Additionally, I would like to extend my thanks to all the faculty members and staff of the PEP department. Their willingness to share knowledge and expertise has greatly enriched my learning experience. Also, I extend special thanks to the Student counsellor, Frau Anja Gatzka whose assistance and support from day one have been invaluable.

Lastly, but most importantly, I extend my heartfelt gratitude to my family. Their unwavering love, support, and belief in my abilities have been the cornerstone of my journey. To my parents, whose sacrifices and encouragement have been the guiding light in my life, I owe an immense debt of gratitude. Their wisdom and values have shaped me into the person I am today, and this achievement is as much theirs as it is mine. To my siblings, thank you for your endless support, understanding, and for always being there to offer a listening ear or a word of advice. Your belief in my dreams has been a constant source of strength and motivation. Balancing the demands of academic research with personal responsibilities can be challenging, but your understanding and encouragement have made this journey smoother and more fulfilling. This thesis is not just a reflection of my efforts but also a testament to the sacrifices, love, and support of my family. I am eternally grateful for everything they have done for me, and I dedicate this achievement to them.

Abstract

Accurate monitoring of NO_2 levels is crucial for air quality management and public health. Satellite-based observations offer extensive coverage but require validation with precise ground-based measurements. The aim of the study is to validate the Global Environmental Monitoring Satellite (GEMS) NO_2 observation products using ground-based Pandora and MAX-DOAS instruments in Seoul and Incheon, South Korea. The primary objective was to evaluate the accuracy and reliability of GEMS tropospheric NO_2 vertical column measurements, comparing them with ground-based observations and the Tropospheric Monitoring Instrument (TROPOMI) data. The analysis utilized data spanning from October 2021 to November 2022, focusing on the hourly, diurnal, weekly, and seasonal variations of NO_2 levels. The study employed a methodical approach, including correlation analyses and bias assessments. The findings revealed a strong correlation between GEMS products among Pandora and MAX-DOAS measurements, with R-values for GEMS operational product vs. Pandora (0.74), GEMS IUP vs. Pandora (0.84), GEMS operational product vs. MAX-DOAS (0.71) and GEMS IUP vs. MAX-DOAS (0.82) indicating moderate to strong positive agreement. Biases were identified; with GEMS operational product overestimating and GEMS IUP underestimating Pandora in Seoul and MAX-DOAS in Incheon NO_2 levels. Hourly, weekly, seasonal and time-of-day analyses indicated that GEMS captured the expected hourly, weekly, seasonal and diurnal variation in NO_2 levels, aligning with Pandora and MAX-DOAS observations. Seasonal variation analysis revealed higher NO_2 levels during colder months, primarily due to increased heating emissions and slower atmospheric chemical reactions that lead to NO_2 accumulation. However, lower NO_2 levels were observed in warmer months, attributed to increased photolysis rates and wet deposition from heavy rainfall. The study also noted distinct diurnal patterns, with peak NO_2 vertical column occurring between late morning and midday, and varied spatially between Seoul and Incheon. The findings of this study highlight the reliability of GEMS in capturing NO_2 variations, demonstrating its ability as a valuable tool for air quality monitoring. However, the identified biases underscore the importance for on-going algorithmic improvements. The study's insights into the spatial and temporal dynamics of NO_2 pollution are crucial for targeted air quality management and public health initiatives in urban and industrial areas.

Keywords: NO_2 monitoring, GEMS instrument, DOAS measurements, air quality, satellite validation, Seoul, Incheon.

Table of Contents

Chapter 1

Introduction

Air pollution is a growing environmental problem in South Korea that is affecting both human health and the ecosystem. The pollution originates from both trans-boundary (South Korea is located in downwind area of China as a result, polluted air from China and dust storms transported by southwest wind impact on South Korea's ambient air pollution levels) (Moon 2021) and domestic activities. The emission of various air pollutants such as nitrogen oxides (NO_x), sulphur dioxide (SO_2), carbon monoxide (CO), Volatile Organic Compounds (VOCs), Ammonia (NH_3), and particulate matter (PM) with an aerodynamic diameter equal to 10µm and 2.5µm (PM_{10} and $PM_{2.5}$) has increased significantly due to industrialization and urbanization. In addition changes in climatic conditions have worsened the air quality in South Korea over the past two decades. According to the study of Leem et al., (2015) air pollution is responsible for 16(% of all deaths in Seoul in 2010 alone. According to the United States National Aeronautics and Space Administration (NASA, 2015), which observed the global air pollution trends from 2005–2014, Seoul is one of the world's most polluted cities. Between 2009 and 2013, the city's mean PM_{10} levels were higher than in many of the world's largest cities including Los Angeles, Tokyo, Paris, and London (Korean National Institute of Environmental Research (NIER), 2015), and is one of the 10 most polluted cities in the world (Gope et al., 2021).

Among these pollutants, NO_x is one of the most significant contributors to air pollution. NO_x refers to a group of reactive gases that include nitrogen oxide (NO) and nitrogen dioxide (NO_2). Exposure to high levels of NO_2 can lead to respiratory problems, particularly in people with asthma, and increase the risk of respiratory infections (Chauhan et al. 2003). It can also aggravate heart disease and cause headaches, nausea, and eye irritation. NO_2 acts as a precursor to the formation of ground-level ozone, which is another harmful air pollutant. NO_2 is particularly important to measure and monitor due to its harmful effects on human health.

The challenging air pollution levels and the need to accurately monitor atmospheric pollutants have led to the constant advancement of environmental remote sensing and data retrieval methods with high level spatial and temporal resolution. The Geostationary Environment Monitoring Spectrometer (GEMS onboard the GeoKOMPSAT-2B) which is the first Ultraviolet-Visible (UV-Vis) spectrometer in geostationary orbit, was launched on February 18, 2020 by the Korean space agency. It is designed to measure total (total = tropospheric + stratospheric) and tropospheric air pollutant columns over Asia in hourly intervals during the

day at spatial resolutions of up to 3.5km × 4km for NO_2 (Kim et al., 2020), enabling the monitoring of local emissions and long-range pollution transport.

The aim of satellite data validation campaigns is to provide independent measurements of the quantities retrieved from the satellite data to assess the quality of the data products. In addition, satellite retrieval algorithms can further be improved by studying the accuracy of the data products and their sensitivity to retrieval parameter choices (Pinardi et al., 2020.). The studies of Boersma et al., (2004); Lin et al., (2015); Lorente et al., (2017); Liu et al., (2019a) as cited in Pinardi et al., (2020) found that tropospheric satellite data products depend on various sources of ancillary data for example, a priori vertical distribution of the absorbing and scattering species, surface albedo and information on clouds and aerosols.

The goal of this study is to validate the results of GEMS tropospheric NO_2 observations products by comparison to the results of tropospheric NO_2 observations from; the MAX-DOAS instrument installed on the roof of the National Institute of Environmental Research (NIER) headquarters in Incheon, the Pandora instrument at Yonsei University Seoul, as well as the Tropospheric Monitoring Instrument (TROPOMI) in the period from October 2021 through November 2022.

1.1.1 NO_2 in the atmosphere

Nitric oxide (NO) and NO_2 are the two nitrogen oxides (NO_x = NO + NO_2) that are relevant for air pollution since NO_2 and NO rapidly convert into each other in the atmosphere.

Sources

NO_x emissions can come from several sources: From natural sources such as lightning, volcanic activity and forest fires. Relevant anthropogenic NO_x emission sources are from internal combustion engines (largely diesel), power plants, heating or electricity generation.

Sinks

NO_2 is lost in the troposphere by reaction with OH, to produce nitric acid

$$M = N_2 \text{ or } M = O_2$$

$$OH + NO_2 + M \rightarrow HNO_3 + M$$

$$HNO_3 + H_2O \rightarrow H^+ + NO_3^-$$

HNO_3 (Nitric acid) is lost through wet deposition when it further reacts with cloud droplets to form nitrate aerosols. (Finlayson-Pitts and Pitts, 2000).

NO_2 can be converted to nitrate by reacting with ozone at night, and further be converted to dinitrogen pentoxide, a reactive nitrogen compound by reacting with nitrate.

$$NO_2 + O_3 \rightarrow NO_3 + O_2$$

$$2NO_2 + 2NO_3 \rightarrow N_2O_5 + 2NO_3$$

Nitrate (NO_3) and dinitrogen pentoxide (N_2O_5) are removed from the atmosphere by wet deposition.

During the day, the Leighton equilibrium describes the relationship between NO_2, NO, and O_3 in the background atmosphere when volatile organic molecules are absent.

$$NO_2 + h\nu \rightarrow NO + O$$

$$O + O_2 + M \rightarrow O_3 + M$$

$$NO + O_3 \rightarrow NO_2 + O_2$$

NO_2 is a pollutant that does not last long in the atmosphere, leading to significant fluctuations in its concentration over time and space. The presence of other air pollutants can also be affected by weather factors such as wind speed, wind direction, and intensity of solar radiation. These factors can either worsen or improve air quality depending on the present weather condition. High pollution concentrations can occur during periods of low wind speed due to accumulation of pollutants in a particular region. While on the other hand, strong winds can carry pollutants far away from a particular region to another region resulting to low pollution concentrations in that particular region.

In summer, the rate of photolysis is high which leads to lower NO_2 in the troposphere, due to a shift in the balance between NO and NO_2 at constant NO_x. However, during winter, the lifetime of NO_2 is longer. The reason is that there is less OH available to react with NO_2 since OH is produced by photolysis. Therefore, the concentration of NO_2 is higher in winter compared to summer. The concentration of NO_2 is inversely related to solar radiation, with higher concentrations during the night and lower concentrations during the day due to photolysis. Thus, a strong diurnal variation is expected, with low NO_2 values at noon and

higher values in the morning and evening. In addition, the emissions from transportation during morning and evening rush hour, diurnal changes of the emission from power plants, and industries are also equally liable for NO_2 diurnal variation.

Exposure to NO_2 can lead to several harmful effects on the respiratory system. When NO_x reacts with ammonia, moisture, and various other compounds, it forms particles, these particles are so small that they can deeply permeate the respiratory tract. A recent study by Meng et al., (2021) shows that there is a direct correlation between short-term exposure to NO_2 and an increased risk of death due to cardiovascular and respiratory issues. Especially prolonged exposure to high levels of NO_2 may contribute to the development of asthma, increasing the risk of respiratory infections and chronic lung disease.

1.2.1 NO_X Spatial distribution In Asia

The spatial distribution of NO_x emissions in Asia has important implications for air quality and public health.

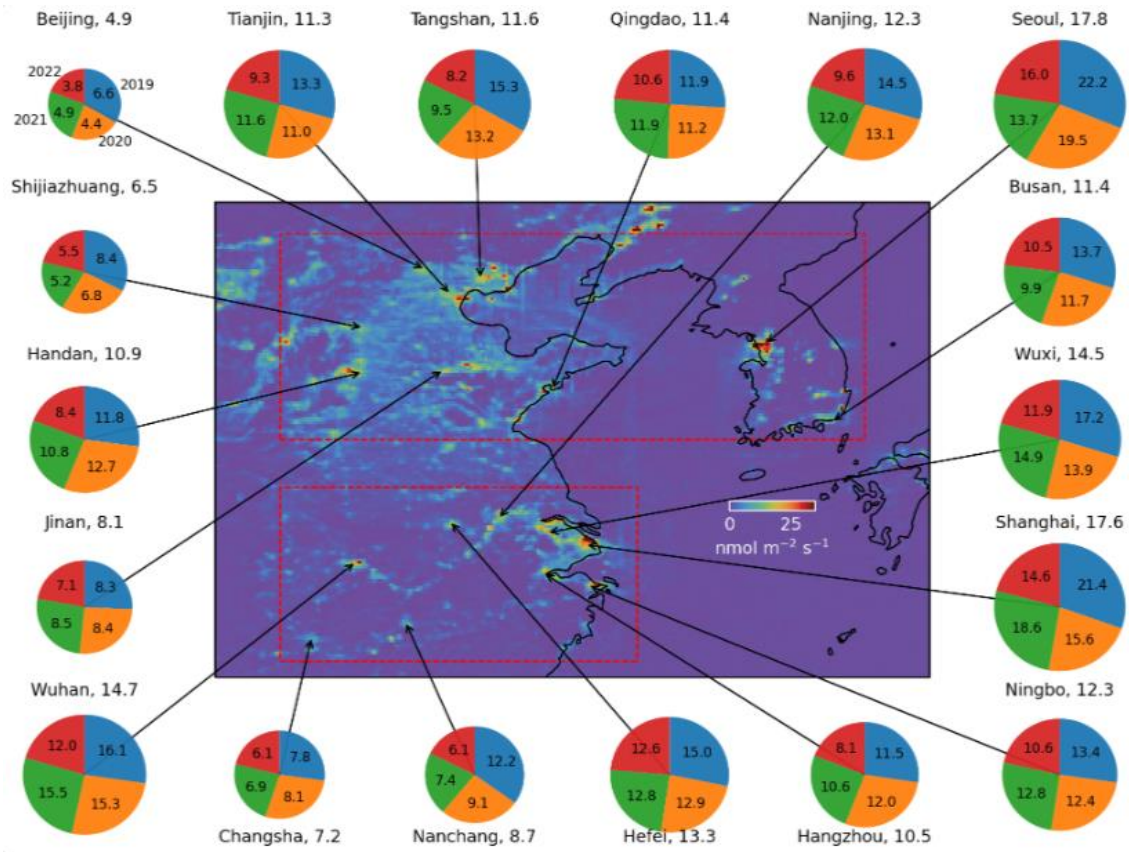

Figure 1.2.1: The central map shows 4-year average NOx emissions throughout the region of East Asia, determined from TROPOMI observations. The annual NO_x emissions in 2019–2022 in cities are displayed as pie

charts. The emission values each year are labelled on or near the corresponding pie slice in nmol m^{-2} s^{-1}. The 4-year average emissions are labelled beside the city names (Adapted from: Lonsdale and Sun 2023).

Figure 1.2.2 shows the NO_x emission distribution in East Asia, according to a study by Lonsdale and Sun (2023) using TROPOMI data. The emissions from individual cities in East Asia are significantly higher than those in North America and Europe. This difference is evident in the enhanced scale of the colour map and pie chart sizes used in the figure. The selected cities in the region of East Asia, particularly in China, show a pattern where the 2022 emissions are generally lower than the 4-year average. In many cases, the emissions in 2022 are also lower than those in 2021 and 2020. This trend is attributed to widespread and stringent measures implemented in China in 2022. Unlike most cities in North America and Europe, where the strongest emissions are typically concentrated in city centres, the highest emissions in selected cities in East Asia are often found in industrial areas or seaports rather than in the urban centres. This spatial distribution indicates a different pattern of NOx emission sources in East Asian cities compared to those in North America and Europe.

The Seoul metropolitan area, as mapped during the Korea–United States Air Quality (KORUS-AQ) campaign, shows high-resolution NO_2 column amounts. Particularly, the west–east extended hotspot in the western part of Seoul is associated with the Incheon industrial complex, while a more south–north extended hotspot is located over central Seoul. Additional emission hotspots are identified near Suwon in the south, which is also an industrialized area. To the northeast of Busan, a hotspot appears to be the port of Ulsan, the largest industrial port in South Korea. Chinese cities generally experienced lower NOx emissions in 2022 than in previous years. This reduction is attributed to direct and indirect impacts of the Omicron variant's spread. However, some cities like Hangzhou, Ningbo, and Jinan showed periods of emission recovery or increase, particularly during the summer and fall of 2020. Shanghai, one of the largest cities studied, had higher NOx emissions than other selected cities, except Seoul. The city saw notable NOx emission reductions during the spring festival in 2019–2021, with 2020 coinciding with initial COVID-19 control measures. Additionally, in 2022, an unprecedented lockdown in Shanghai due to the Omicron variant led to further reductions in NOx emissions.

1.3.1 Study area

The study area for this research is Seoul, the capital city of South Korea. Seoul is located in the north-western part of South Korea and covers an area of 605.21km^2. It has a population of

approximately 10 million people, making it the largest city in South Korea and the fourth-largest metropolitan area in the world. Seoul is located in a basin surrounded by mountains, which can lead to poor air quality due to the accumulation of pollutants. The city is also affected by trans-boundary pollution transport from neighbouring countries, particularly China, which can have a significant impact on air quality (Wikipedia). The MAX-DOAS instrument used in this study was situated in Incheon which is about 25km west of Seoul capital city and part of the Seoul metropolitan area.

South Korea have made significant efforts to improve air quality in recent years, with the introduction of various policies and regulations to reduce emissions from vehicles, power plants, and other sources. Despite these efforts, air pollution remains a major issue in Seoul, particularly during the winter months when the city experiences high levels of particulate matter (PM) and NO_2 (Ngarambe et al., 2021).

1.4.1 Weather pattern in South Korea

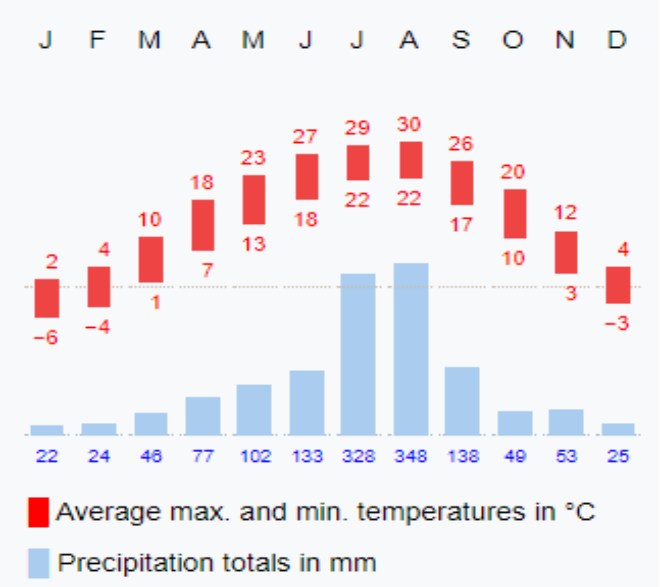

Figure 1.4.1: Climate in South Korea (https://en.wikipedia.org/wiki/Seoul#Geography)

South Korea experiences a wide range of temperatures throughout the year. Summers are hot and humid, with average high temperatures ranging between 25°C to 30°C, while winters are cold, with average lows ranging from -5°C to 5°C, occasionally dropping below freezing. In Seoul, the summer temperatures are hot and humid, averaging between 28°C to 30°C, but winters are colder, with average lows falling between -6°C to -10°C. The country receives a significant amount of rainfall, especially during the summer monsoon season from June to

September, with annual averages between 1,000mm to 1,500mm. In Seoul, rainfall is more evenly distributed throughout the year, but high during the summer, averaging around 1,300mm annually. Humidity levels in South Korea are generally high, particularly in the summer months, ranging from 70% to 90%. Seoul experiences similar humidity levels, often exceeding 70% during summer. Regarding the seasons, spring in South Korea is characterized by mild temperatures between 10°C to 20°C. Autumn also sees mild temperatures in a similar range. This type of weather pattern is very important for the satellite instrument observation such that it results to changes in sensitivity to ground level tropospheric NO_2 in the different seasons. The forthcoming analysis section of this study will include a crucial discussion on this matter.

Chapter 2

DOAS measurement technique

Differential Optical Absorption Spectroscopy (DOAS) is a remote sensing technique used to measure trace gas concentrations in the atmosphere, including nitrogen dioxide (NO_2). It is employed both for the GEMS satellite data and the analysis of the ground-based MAX-DOAS and Pandora measurements.

DOAS is classified into active and passive types based on light sources. Active DOAS utilises artificial light source e.g., Xe-arc lamps to determine average surface concentrations of trace gases (O_3, NO_2, HONO, SO_2, BrO, IO, and OClO) (Zhou, et. al., 2009). Passive DOAS on the other hand relies on natural light sources such as the sun, moon, or stars to measure the trace gas columns. The main principle of the DOAS technique is based on the Lambert Beer's law of absorption which involves measuring the amount of light absorbed by atmospheric gas constituents at specific wavelengths. The absorption spectrum of a gas is unique, so by measuring the amount of light absorbed at different wavelengths, the concentration of the gas can be determined.

Method

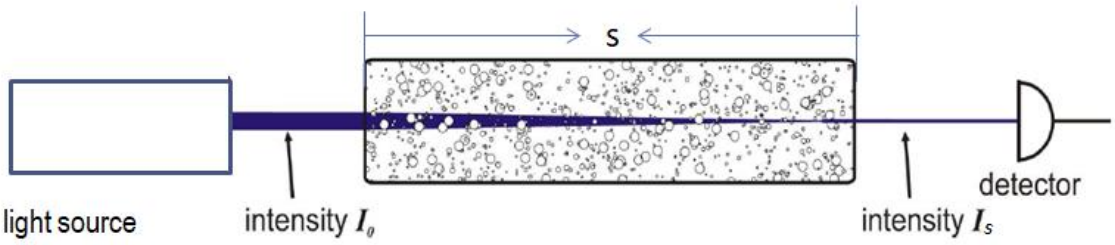

Figure 2.1: principle of absorption spectroscopy of trace gases. A light source with initial intensity (I_0), that passes through a trace gas cell with length (s) containing the absorbing molecules. As the light interacts with the gas, some of it is absorbed, reducing the intensity of the light that reaches the detector on the other side, measured as I_S. The difference in intensity is used to calculate the concentration of the absorbing species according to Beer-Lambert Law. (Adapted from, University of Bremen practical environmental measurement techniques, Institute of Environmental Physics (IUP). Supervised by, Midhun George and M. D. Andrés Hernández. Rayleigh scattering of standard molecules using Cavity Ring-Down Spectroscopy Last revised on 01.03.2019)

In a uniform medium, where light intensity decreases as a result of absorption by molecules, the change in intensity (dI) over a small path length (ds) is proportional to the product of the

concentration of absorbers (ρ_A), the absorption cross-section (σ_A), and the present intensity of light (I_S).

$$dI = -\rho_A \sigma_A I \, ds \qquad (1)$$

The decrease in light intensity is accounted for by (-) in equation (1)

By integrating equation (1), we can find the relationship between the initial intensity I_0 and the intensity I after traveling a distance s through the medium

$$\ln\left(\frac{I_{(s)}}{I_o}\right) = -\sigma_A \int_0^s \rho_A ds \qquad (2)$$

This yields the exponential form of Lambert Beer's law.

$$I(s) = I_0 \exp\{-\sigma_A \rho_A s\} \qquad (3)$$

Where:

- I(s) is the light intensity after traveling through the medium.
- I_0 is the initial light intensity.
- ρ_A is the concentration of absorbing molecules.
- σ_A is the absorption cross-section of the absorbers.
- S is the path length through the medium.

However, we also have to include light extinction due to scattering into equation (3) because both absorption and scattering take place in the atmosphere. There are two main types of scattering in the atmosphere, which are Rayleigh and Mie scattering.

Rayleigh scattering: The foundational work on Rayleigh scattering was first introduced by Lord Rayleigh (Strutt, 1871), this scattering phenomenon occurs when light is scattered on particles smaller than the wavelength of light. Molecules like nitrogen and oxygen are typical examples that demonstrate this type of scattering for visible light. Rayleigh scattering is elastic, meaning the energy of the scattered light remains unchanged. Its occurrence depends on factors such as the size and composition of the scattering particles and the light's wavelength. The most commonly used expression to quantify Rayleigh scattering is the Rayleigh scattering cross-section formula given by

$$\sigma_{Ray} = \frac{8\pi^3\left(n^2-1\right)^2}{3\rho_A^2 \lambda^4} \qquad (4)$$

Where:

n is the refractive index of the medium

λ is the wavelength of the incident light in the medium.

The term $n^2 - 1$ is squared, and the whole expression is divided by λ^4 indicating the strong inverse dependence on the fourth power of the wavelength.

$$\sigma_{Ray} \propto \lambda^{-4} \qquad (5)$$

In this type of scattering, shorter wavelengths are scattered more than longer wavelengths causing the sky colour to appear blue.

The phase function of Rayleigh scattering, describing the probability of scattering as a function of scattering angle is given by:

$$P(\theta) = \frac{3}{4}\left(1 + cos^2(\theta)\right) \qquad (6)$$

Where:

$P(\theta)$ is the phase function indicating that the forward and backward scattering is most effective when θ is 0 or 180 degrees ($cos^2(\theta) = 1$) and least effective at 90 degrees to the incident light ($cos^2(\theta) = 0$) then $P(\theta)$ has a minimum value of $\frac{3}{4}$.

$cos^2(\theta)$ account for the change of scattering with the angle.

θ is the angle between the direction of the incoming light and the direction of the scattered light.

Mie scattering: This type of scattering occurs when light interacts with particles that are about the same size as, or larger than, its wavelength. Mie scattering of visible light is typically observed with cloud droplets and aerosol particles. It was first described by Gustav Mie in 1908, this phenomenon allows light to scatter in all directions when it encounters such particles (Mie, 1908). Mie scattering leads to several distinctive optical effects. These include the generally white or grey appearance of clouds (due to the near-equal scattering of all visible light wavelengths), the formation of halos around the Sun or Moon, the creation of glory and coronas around light sources, and a decrease in visibility in cases of pollution or mist. Mie scattering also contributes to the overall brightness and colouration of the sky under different atmospheric conditions, including overcast skies, and plays a role in the colour changes observed at sunrise and sunset.

In Mie scattering, there is less wavelength dependence. Instead, the size of the aerosol particles (the aerosol size parameter) majorly determines the characteristics of the scattering. This includes both the direction and intensity of the scattered light. The phase function for Mie scattering is more complex than that for Rayleigh scattering due to the larger size of the

scattering particles and is highly dependent on how the sizes of the particles are distributed and refractive index or composition of these particles.

$$\sigma_{\text{Mie}} \propto \lambda^{-k} \qquad (7)$$

Where $k = 0....2$

We can then add the extinction cross section caused by molecular absorption, Rayleigh scattering and Mie scattering into equation (3)

$$I(s) = I_0 \exp\{-\sigma_A \rho_A s - \sigma_{Ray} \rho_{Ray} s - \sigma_{Mie} \rho_{Mie} s\} \qquad (8)$$

σ_{Ray} *and* ρ_{Ray}: Rayleigh scattering cross-section and the concentration of Rayleigh scatterers, respectively for particles much smaller than the wavelength of light.

σ_{Mie} *and* ρ_{Mie}: Mie scattering cross-section and concentration of Mie scatterers, respectively for particles having sizes equal to or larger than the wavelength of light.

Considering that there are various different absorbers in the atmosphere with wavelength dependence and characteristic absorption spectrum, equation (8) yields the equation for light absorption in an homogeneous medium with N absorbers

$$I(s, \lambda) = I_0(\lambda) \exp\{-\sum_{i=1}^{N} \sigma_{Ai}(\lambda) \rho_{Ai} s - \sigma_{Ray}(\lambda) \rho_{Ray} s - \sigma_{Mie}(\lambda) \rho_{Mie} s\} \qquad (9)$$

Next, we consider an inhomogeneous medium where concentration of absorbers is changing along the light path (ds).

Using the slant column (SC) of the absorber which is defined as the total amount of the absorber per unit area integrated along the light path, ds through the atmosphere,

$$SC_i = \int_0^{TOA} \rho_{Ai} ds \qquad (10)$$

Substituting into equation (9) yields

$$I(s, \lambda) = I_0(\lambda) \exp\{-\sum_{i=1}^{N} \sigma_{Ai}(\lambda) SC_i - \sigma_{Ray}(\lambda) SC_{Ray} - \sigma_{Mie}(\lambda) SC_{Mie}\} \qquad (11)$$

Next, the scattering contributions from Rayleigh and Mie are approximated by a low order polynomial in Equation (9)

$$\sigma_{Ray}(\lambda) SC_{Ray} + \sigma_{Mie}(\lambda) SC_{Mie} = \sum_{j=0}^{M} p_j \lambda^j \qquad (12)$$

The polynomial is needed in order to balance the scattering effect.

Therefore, Equation (11) yields.

$$I(s, \lambda) = I_0(\lambda) \exp\left\{-\sum_{i=1}^{N} \sigma_{Ai}(\lambda) SC_i - \sum_{j=0}^{M} p_j \lambda^j\right\} \quad (13)$$

Taking the natural logarithm of equation (13), the result is a linear equation between the differential optical depth, the slant columns of the absorbers and a polynomial.

This is known as the DOAS equation:

$$\ln\left(\frac{I(\lambda)}{I_o(\lambda)}\right) = \left\{-\sum_{i=1}^{N} \sigma_{Ai}(\lambda) SC_i + \sum_{j=0}^{M} p_j \lambda^j\right\} \quad (14)$$

When Equation (14) is solved for many discrete wavelength ranges, $\lambda_1, \lambda_2 \ldots, \lambda_n$ we have many equations for the same slant column (SC_i) and polynomial coefficients (p_j). To solve the many equations problem, we use a standard linear least squares fit method to find the set of SC_i and p_j values that best fits all measurements across the various wavelength ranges.

What is needed is the vertical column (*VC*), which is the total number of molecules in a column of air extending vertically from the Earth's surface to the top of the atmosphere (TOA).

To be able to obtain the *VC*, the Air Mass Factor (*AMF*) is used to convert the *SC* to *VC*. It accounts for the angle of the light path through the atmosphere, which affects the actual path length of the light. The *VC* is then calculated as follows:

$$\text{AMF} = \frac{SC}{VC} \quad (15)$$

Then, the tropospheric NO_2 *VC* is derived by dividing the observed NO_2 slant column *SC* by the AMF.

$$VC = \frac{SC}{\text{AMF}} \quad (16)$$

2.1.1 Satellite measurement of tropospheric NO_2 vertical column

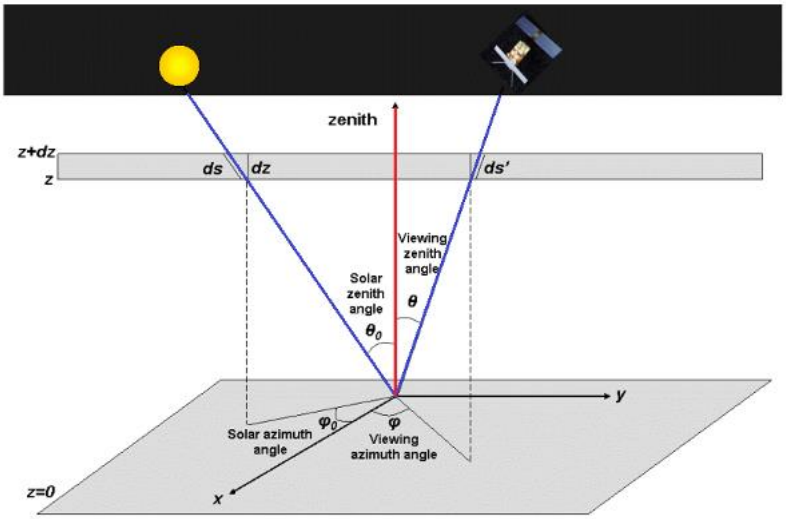

Figure 2.1.1: Sketch of satellite radiation measurement and geometry in a plane parallel atmosphere. The blue lines are the optical path relevant to the slant column density (first step of the DOAS algorithm). The red line is relevant to the vertical column density (second step of the DOAS algorithm). (Adapted from: ESA Sentinel online, 2023).

Tropospheric NO_2 can be measured using satellite instruments that detect reflected sunlight in the ultraviolet and visible ranges in viewing nadir geometry, (downward-looking) pointing towards the Earth's surface. Satellite instruments that measure NO_2 and other atmospheric constituents detect the number of molecules between the instrument and the Earth's surface. Satellite instruments measure the total column of atmospheric constituents using the DOAS principle (Richter A., 2006, p. 1).

However, the vertical sensitivity of satellite observations can be influenced by a number of atmospheric factors including; the vertical distribution of NO_2, surface reflectance (albedo), clouds, sun geometry, satellite geometry, aerosols and retrieval algorithm.

When there is heavy cloud cover, it is not possible to derive NO_2 concentration near the surface below the clouds from satellite observations; this reduces the sensitivity of these instruments and introduces a fair weather bias in satellite observations. When there is a cloud, the sensitivity to NO_2 below the cloud is nearly zero. However, within the cloud, the path length of photons can be increased due to scattering by cloud particles resulting in more NO_2 being absorbed, consequently increasing the sensitivity of the measurement within the cloud. Above the cloud, the increased reflectance from the cloud tops (which act as a bright

background) can increase NO_2 absorption, hence increasing the sensitivity of the satellite observations compared to a cloud-free case.

NO_2 concentration is higher close to the ground due to emissions from traffic, industrial activities, and other combustion processes. In the absence of clouds, a satellite instrument can have good sensitivity to this higher concentration close to the ground, in particular if surface reflection is not too low. The atmospheric boundary layer (ABL), which is about 1km above the surface depending on topography and vertical mixing, is where most of the NO_2 is present. Satellite instruments are mainly sensitive to NO_2 concentrations within the ABL because of their large size. Above the ABL, NO_2 concentrations decrease rapidly and satellite instruments are less sensitive due to the lower amounts of NO_2. The sensitivity in the lower stratosphere is relatively good because NO_2 concentrations can be significant due to the longer lifetimes of gases at those altitudes. As satellite instruments measure the total column of NO_2, depending on study interest, the stratospheric and tropospheric NO_2 column density are separated from the total column density using complex and advanced retrieval algorithms for this process.

2.2.1 Satellite Instruments measuring NO_2 in the atmosphere

The Scanning Imaging Absorption Spectrometer for Atmospheric CHartographY (SCIAMACHY), was operational from March 1, 2002, to April 12, 2012, it was mounted on the polar, sun-synchronous, low Earth orbit (LEO) platform of the first European Polar Earth Observation Mission (POEM-1), known as ENVISAT (Burrows et al., 1995). SCIAMACHY's wavelength range spanned 240–2380 nm, covering the ultraviolet, visible, and near-infrared (UV/visible/NIR) spectra with a spectral coverage of 0.20–1.50 nm (Bovensmann et al., 1999; Piters et al., 2006). It featured a spatial resolution of 3 x 132 km in limb vertical and 32 x 215 km in nadir horizontal resolution, enabling global coverage within a three-day cycle at the equator. SCIAMACHY was designed to carry out atmospheric trace gases observations from the troposphere up to the mesosphere in a continuous full cycle orbit.
The Ozone Monitoring Instrument (OMI) on board the Aura satellite was launched by NASA in 2004 (Levelt et al., 2018). OMI has a high spatial resolution of 13 x 24 km^2 at nadir and measures tropospheric NO_2 columns with an accuracy of about 20-30% (Boersma et al., 2018).
Another satellite instrument used for monitoring tropospheric NO_2 is the TROPOspheric Monitoring Instrument (TROPOMI), which was launched in 2017 on board the Sentinel-5

Precursor (S5P) satellite by the European Space Agency (ESA). TROPOMI has a high spatial resolution of 3.5 x 5.5 km^2 and measures tropospheric NO_2 columns with an accuracy of about 10-20% (Veefkind et al., 2015). More of these satellite instruments are presented in the table below.

Table 1: NO_2 measuring satellite Instruments and their specifications

Satellite	**Instrument**	**Launch Year**	**Spatial Resolution**	**Orbit**	**Global Coverage**	**Bands**	**Channels**
ERS-2	GOME	21.04.1995 - July 2011	40 x 320 km^2	Sun-synchronous, polar (LEO)	3 days	4	4096, 3 polarization
Envisat	SCIAMACHY	01.03.2002-12.04.2012	30 x 60 km^2	Sun-synchronous, polar (LEO)	6 days	8	8192, 7 polarization
Aura	OMI	15.07.2004	13 x 24 km^2	Sun-synchronous, polar (LEO)	1-2 days	2	
Metop-A, B, C	GOME-2	19.10.2006	40 x 80 km^2	Sun-synchronous, polar (LEO)	1 day	4	4096, 200 polarization
Suomi NPP	OMPS	October 2011	50 x 50 km^2	Sun-synchronous, polar (LEO)	1 day		
Sentinel 5p	TROPOMI	13.10.2017	3.5 x 5.5 km^2	Sun-synchronous, polar (LEO)	1 day		
GEO-KOMPSAT-2B	GEMS	18.02.2020	3.5 x 4 km^2	GEO	Asia, hourly		
Intelsat 40e	TEMPO	April 2023	2 x 4.5 km^2	GEO	North America, hourly		
MTG-S1	Sentinel-4	2024	8 x 8 km^2	GEO	Europe, hourly		

2.3.1 GEMS

The Geostationary Environment Monitoring Spectrometer (GEMS) onboard the GEO-KOMPSAT-2 (GK2B) satellite is a Korean satellite mission launched on February 18 2020 to monitor air quality in Asia in near-real-time. The satellite which is positioned in geostationary orbit at 128.2 degrees east longitude was developed by the Korea Aerospace Research Institute (KARI) and the National Institute of Environmental Research (NIER) in Korea, in collaboration with the National Aeronautics and Space Administration (NASA) and the

National Oceanic and Atmospheric Administration (NOAA) in the United States. GEMS is equipped with a UV-VIS (ultraviolet-visible) spectrometer that measures the columns of various trace gases in the atmosphere, including NO_2, O_3, SO_2, HCHO. The spectrometer covers a spectral range from 300 to 500 nm with a spectral resolution of 0.5 nm and a spatial resolution of 3.5 km x 4 km. The DOAS principle in Platt and Stutz (2008) is applied to the GEMS NO_2 column retrieval. The ability of GEMS to take hourly observations of NO_2 (up to 9 times per day) during daytime, and as the first satellite instrument to carry out such observation from geostationary orbit (Lee et al., 2021), differentiates it from the other satellite instruments measuring NO_2.

2.3.2 GEMS products

Two different level two (L2) GEMS tropospheric NO_2 products were used in this study: GEMS NIER version 2.0 (operational product) and GEMS IUP version 0.9 (IUP product)

GEMS operational product

In the GEMS operational product, the NO_2 slant columns are retrieved in the spectral range of 400–434 nm using the DOAS method. Next, the slant columns are separated into their stratospheric and tropospheric slant columns by applying the filtering method described in Bucsela et al., (2013). The conversion of tropospheric vertical columns from the tropospheric slant column is done by using the tropospheric AMF using a look up table (LUT) applying the surface Lambertian equivalent reflectivity from the GEMS surface product version 2.0 (GEMS surface LER V2.0). The GEMS operational product applies corrections for clouds and aerosols. A priori information on NO_2 and aerosol distributions are taken from the GEOS-chem mode, a three-dimensional global tropospheric chemistry transport model used to model trace gas and aerosol concentrations (Kim et al., 2015).

GEMS IUP product

The GEMS IUP product retrieves NO_2 slant columns in the fitting window of 405–485 nm using the DOAS method. Next, the slant columns are separated into their stratospheric and tropospheric parts by applying a modified version of the STRatospheric Estimation Algorithm from Mainz (STREAM) method (Beirle et at., 2016) called Stream-B. The conversion of tropospheric vertical columns from the tropospheric slant column is done by using a tropospheric AMF LUT applying OMI minimum LER climatology. A priori data on NO_2 is taken from the Tracer Model version 5 (TM5) model which is used in the TROPOMI

processor (Williams et al., 2017). There are no corrections for clouds or aerosols for this version of the GEMS IUP product.

2.4.1 TROPOMI product

The TROPOMI product, the NO_2 slant columns are retrieved in the spectral range of 405–465 nm using the DOAS method. Next, the slant columns are separated into their stratospheric and tropospheric parts by applying the TM5 assimilation system method. The conversion of tropospheric vertical columns from the tropospheric slant column is done by using the tropospheric AMF LUT provided by TROPOMI Sentinel 5P directionally dependent Lambertian equivalent reflectivity (S5P DLER). A priori data on NO_2 is taken from the TM5 model. The TROPOMI product applies corrections for clouds but no corrections for aerosols.

Chapter 3

Ground-based tropospheric NO_2 vertical column datasets

In this study, two ground-based instruments, a Multi-Axis Differential Optical Absorption Spectroscopy (MAX-DOAS) instrument and a Pandora instrument were used validation instruments. The NO_2 column retrieval from the ground-based instruments is also based on the DOAS principle (Platt and Stutz 2008).

3.1.1 Zenith sky measurement geometry

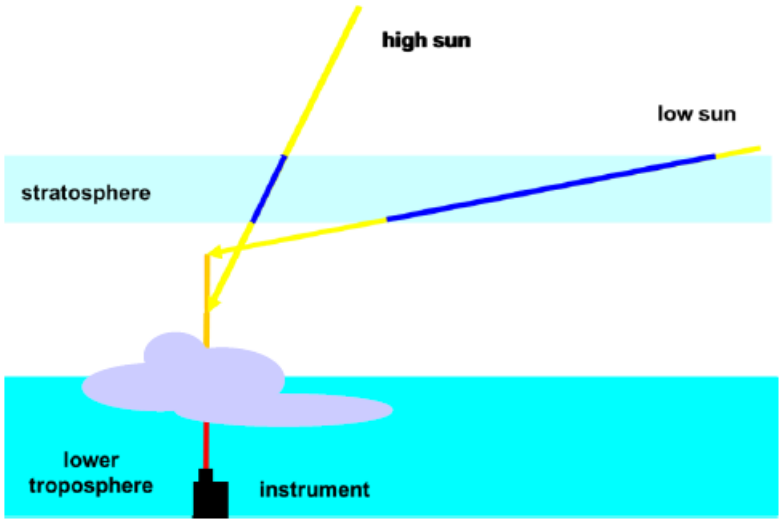

Figure 3.1.1 Stratospheric Observations (zenith-sky DOAS) viewing geometry. Adapted from: IUP University of Bremen, DOAS webpage. Available at: https://www.iup.uni-bremen.de/doas/maxdoas_instrument.htm (last accessed: 11 November 2023)

Zenith sky viewing geometry is characterized by light scattering high above the instrument, are highly effective for measuring stratospheric NO_2, particularly during twilight. In this geometry, the light path is relatively short through the troposphere but extends significantly through the stratosphere. At low sun angles, such as during twilight, the light path through the stratosphere becomes longer. Additionally, the presence of clouds does not change the light path in the stratosphere. The AMF can be approximated as a function of the solar zenith angle (SZA) using the relation $1/\cos(\phi)$.

Therefore, $AMF = \frac{SC}{VC} = \frac{1}{\cos(\phi)}$ (17)

However, at SZA=90° the *AMF* becomes infinity. An effective approach to solve this problem is to use more complex models or algorithms called the Radiative Transfer Models (RTMs) that can provide the *AMF* at high SZA values. These models take into account the scattering properties of the atmosphere, that light path is limited in the spherical atmosphere and taking average of the total light path to provide estimate of the *AMF* under these conditions.

3.1.2 Off-axis measurement geometry

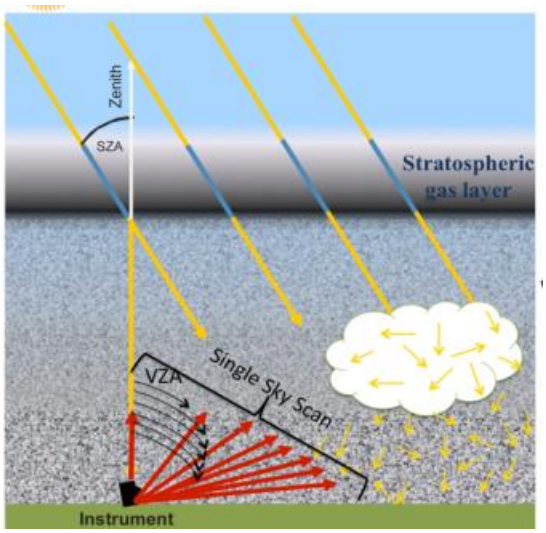

Figure 3.1.2 Demonstration of the MAX-DOAS principle: side view . Simplified photon paths through the atmosphere are shown in yellow. A single sky scan sequence for profile retrieval consists of multiple viewing zenith angles (VZAs) in a specific direction (viewing azimuth angle, VAA) at a specific solar zenith angle (SZA) and is shown in red (Adapted from Dong et. al., 2020).

Off-axis DOAS measurements are effective for measuring tropospheric constituents like NO_2 due to the fact that: they have long light paths through the lower troposphere, maintain a constant light path through the stratosphere, and show a small dependence on the sun's position. As the instrument is pointed lower, the light path gets longer, enhancing tropospheric sensitivity.

Additionally, the AMF can also be approximated as a function of the elevation angle using the relation 1/sin (ϕ).

Therefore, $AMF = \frac{SC}{VC} = \frac{1}{\sin(\phi)}$ (18)

$\frac{1}{\sin(\phi)}$ Implies that as the elevation angle decreases (i.e., the instrument is pointed closer to the horizon), the light path through the atmosphere becomes longer, particularly through the

lower troposphere. However, in this type of measurement geometry, the presence of cloud significantly changes the light paths.

As we have discussed so far in chapter 2, $I_0\ (\lambda)$ is the intensity of the light source before absorption by molecules hence taken as the reference spectrum. However, a complication for ground based MAX-DOAS measurements is that it cannot measure the extra-terrestrial spectrum, $I_0(\lambda)$, directly. Thus a measurement taken towards the zenith sky (looking upward from the ground) is used as $I_0(\lambda)$. This is because the zenith sky measurement is less sensitive to trace gases in the lower troposphere hence the reference spectrum will have low absorption of these species. For off-axis measurements, the smaller the elevation angle, the higher the sensitivity to absorbers in the boundary layer. Similar to the MAX-DOAS measurements, the Pandora instrument carries out zenith sky and off-axis measurements to retrieve total column of atmospheric constituents in this case NO_2. Direct sun measurements are used to extrapolate an extra-terrestrial spectrum $I_0(\lambda)$, which usually is substituted as the reference spectrum to calculate the slant column.

3.2.1 MAX-DOAS product

The MAX-DOAS instrument measures scattered sunlight at different elevation angles and wavelengths, allowing for the retrieval of the vertical distribution of NO_2 and other atmospheric constituents (Hönninger et al., 2014). However, in this study, only tropospheric columns are used, derived with the geometrical approximation as discussed in section 3.2.2. MAX-DOAS observations can be performed under daylight conditions, and below clouds. From the MAX-DOAS perspective, clouds also have a shielding effect to NO_2 above the cloud; this is most often only a small part of the tropospheric NO_2 column, because tropospheric NO_2 primarily resides in the ABL below the cloud.

3.2.2 MAX-DOAS instrument setup and data preprocessing

A MAX-DOAS instrument consists of a telescope, a grating spectrometer with a CCD detector, a fibre optics cable (quartz) between spectrometer and telescope and a computer for data acquisition analysis.

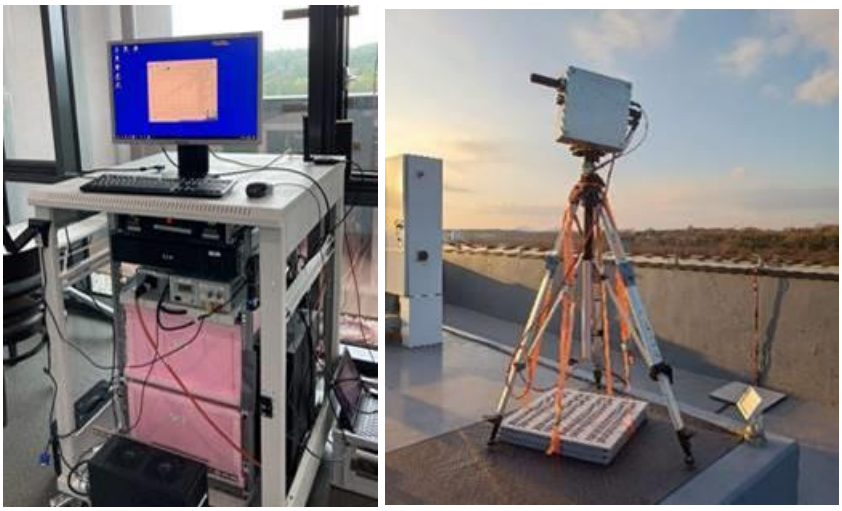

Figure 3.2.2: The MAX-DOAS telescope unit (right) as installed on the roof of the National Institute of Environmental Research (NIER) headquarters Incheon with coordinates (37.57°N, 126.64°E). On the left is the instrument and a computer to visualize the output data inside the building. (Photo by Andreas Richter, IUP)

Telescope: The telescope in the MAX-DOAS instrument is used to collect the scattered light from different azimuthal and elevation angles in the sky (hence Multi Axis). The telescope is located on the roof of the building and is connected to the spectrometer in the lab via fibre optics cable.

Grating Spectrometer: This is the main component of the instrument used for dispersing light into its spectrum. The atmospheric gases that absorb light at specific wavelengths are separated at different wavelengths of light using the grating spectrometer.

CCD Detector: A Charge-Coupled Device (CCD) detector is used to capture the dispersed light spectrum from the grating spectrometer whereby it converts the light into an electronic signal which is then measured and analysed.

Fibre Optics Cable (Quartz): This cable connects the telescope to the spectrometer. It is made of quartz to efficiently transmit UV and visible light without significant loss, ensuring accurate spectral data is sent from the telescope to the spectrometer.

Computer for Data Acquisition and Analysis: The computer processes the electronic signals from the CCD detector, converting them into spectral data. From the computer, the instrument can be controlled and the data collected can also be analysed to determine the concentration of various atmospheric constituents.

The MAX-DOAS instrument installed on the roof top of NIER headquarters Incheon is a 2 (dual) channel instrument (UV + VIS, 300–370nm and 400–530nm). In the UV channel, it has a Full Width at Half Maximum (FWHM) of 0.5nm, and 0.65nm FWHM in the VIS

channel. Measurements were taken in five azimuthal directions (137.5, 170, 185, 266.5, 340°) and nine elevation angles (1, 2, 3, 4, 5, 6, 8, 15, 30°).

MAX-DOAS tropospheric NO_2 slant column dataset were provided by Andreas Richter, IUP Bremen. The data is first filtered to include only those measurements made at a specific line of sight angle (105°, 15° above the horizon), which is the viewing zenith angle.

The Air Mass Factor (AMF) for a zenith angle of 15° is determined from the geometrical approximation:

$$AMF = \frac{1}{SIN(VZA)} - 1$$

$$AMF\ (VZA = 15°) = \frac{1}{SIN(15°)} - 1 = 2.864.$$

The Vertical Column (VC) is then converted from slant column by using this geometric approximation; this is based on the idea assumption that there is only one light path with a single scattering event.

3.3.1 Pandora product and preprocessing

The Pandora instrument has a similar setup like the MAX-DOAS instrument. The Pandora is a passive UV-visible hyper spectral sensor with a two-dimensional charge-coupled device (CCD) and a 1.6° FOV. The spectral resolution and its sampling interval are 0.6 FWHM and 0.23 nm, respectively. Pandora at Yonsei University has been providing measurement of NO_2 since 2012 (Park et al., 2019). From the direct sun measurements, the total column NO_2 from Pandora is retrieved through the DOAS technique (Herman et al., 2009) within the spectral window of 370 to 500 nm.

For this study, the Level 2 Pandora total column data used for the analysis were obtained from the Pandonia Global Network (PGN) website. The specific dataset can be accessed via the following link: https://data.pandonia-global-network.org/Seoul/Pandora54s1/L2/Pandora54s1_Seoul_L2_rnvs3p1-8.txt (last accessed on 10 October 2023). The dataset was filtered for measurements between October 1, 2021, and November 30, 2022. The next step taken was to convert the default unit of total NO_2 column

from moles per square meter to molecules per square centimetre using Avogadro's number. Finally, times were converted to the local time zone of Seoul.

To obtain the tropospheric NO_2 from the Pandora total column (tropospheric + stratospheric), we make use of the TM5 model. This model separates tropospheric and stratospheric vertical column densities from the total vertical column measured by the instrument (Vincent et al., 2010). The stratospheric TM5 model columns were interpolated to match time of measurements of the Pandora dataset. This interpolation was performed using a linear interpolation method. The resulting interpolated TM5 values were assigned to a new column labelled "Interpolated values" within the Pandora total column dataset, ensuring that the data points align in time. Then, the difference between the values in "NO_2 total vertical column amount" column of the Pandora data and the corresponding values in the "Interpolated values" column is computed. These differences are stored in a new column labelled "NO_2 tropospheric vertical column"

From the Pandora data dataset caveat, column 36 provides information on the quality of the measurement values. Quality level 10 (high quality) was selected in filtering for measurement data quality. This process isolates and gathers data points characterized by potentially high confidence or assurance within the dataset for further analysis.

Chapter 4

Previous studies on validation of satellite observations using ground-based measurements

Several validation studies have been conducted with ground-based measurements. For example, Irie et al. (2008) carried out Validation of OMI tropospheric NO_2 column data using MAX-DOAS measurements deep inside the North China Plain in June 2006. They found that the MAX-DOAS measurements provided valuable information about the spatial distribution of NO_2, which could not be captured by satellite measurements alone. When MAX-DOAS and OMI measurements of tropospheric NO_2 columns were compared, it was discovered that OMI data from the Aura satellite may have a positive bias of $1.6x10^{15}$ molecule cm^{-2} (equivalent to 20%). However, this bias falls within the OMI data's uncertainty range. When these findings were combined with validation findings from the United States, Europe, and the Pacific Ocean, it was suggested that a bias of +20% to -30% was a reasonable estimate, taking into account regional differences.

Another validation study was conducted by Verhoelst et al., 2021 using MAX-DOAS measurements. The NO_2 column measurements from TROPOMI were compared to those from 19 Multi-Axis Differential Optical Absorption Spectroscopy (MAX-DOAS), 26 Network for the Detection of Atmospheric Composition Change (NDACC) Zenith-Scattered-Light DOAS (ZSL-DOAS), and 25 Pandonia Global Network instruments. The comparison revealed that the TROPOMI data exhibited a negative bias for tropospheric column data, ranging from -23% to -37% in clean to slightly polluted conditions but up to -51% in highly polluted areas; approximately -2% in summer to -15% in winter; and a bias ranging from zero to -50% for total column data, depending on total NO_2 column magnitude, with small to slightly positive biases for columns less than 6.0×10^{15} molecules cm^{-2}.

In the study of Kim et. al., (2023) conducted at four sites in Seosan, South Korea, from November 2020 to January 2021. The GEMS Level 2 NO_2 vertical column version 1.0 available immediately after the in-orbit test in July 2020 was used. Correlation coefficients between GEMS and Pandora NO_2 data ranged from 0.35 to 0.48, with a correction for cloud condition less than 0.7. Better correlation coefficients of 0.62 to 0.78 were found with a correction for cloud condition less than 0.3, indicating higher sensitivity of GEMS to atmospheric NO_2 in less cloudy conditions.

The present study aims at validating the GEMS NO_2 product using MAX-DOAS and Pandora NO_2 products in Seoul, South Korea from 1 October 2021 to November 2022

4.1.1 Ground based instrument locations

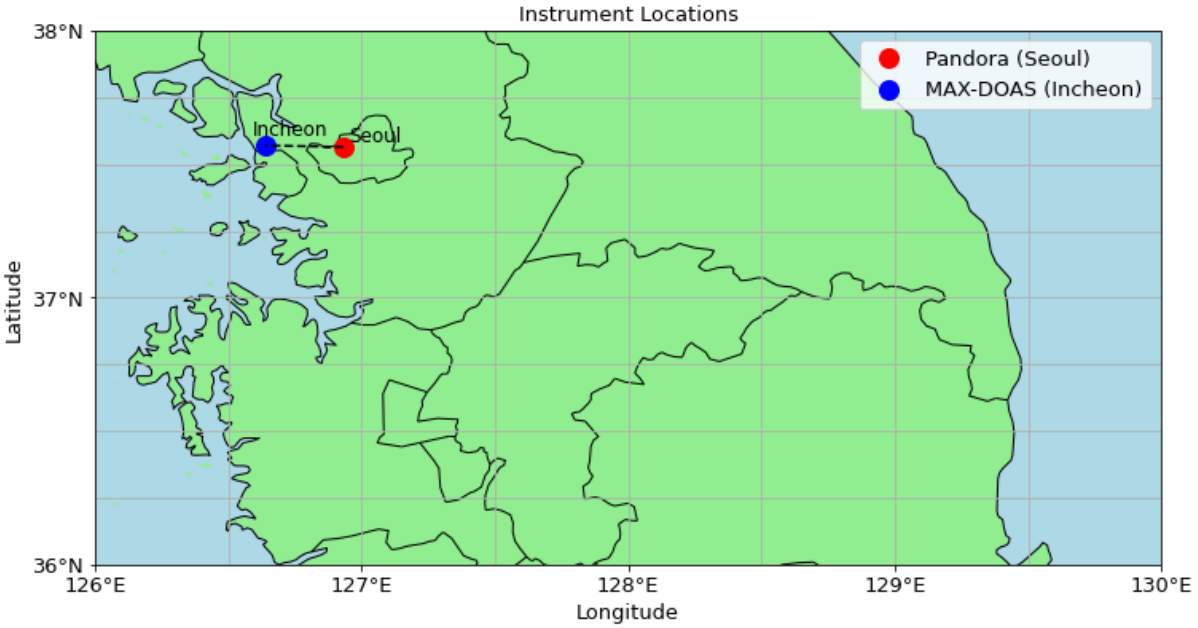

Figure 4.1.1 Locations of the ground based instruments; MAX-DOAS (37.57°N, 126.64°E) and Pandora (37.5644°N, 126.9340°E) in Incheon and Seoul respectively.

The need for validation of GEMS satellite measurements led to the GEMS MAP of Air Pollution 2021 (GMAP2021) campaign from 10 October to 25 November 2021 (Kim, et al., 2023) and the Satellite Integrated Joint monitoring of Air Quality campaign 2022(SIJAQ2022) from 2 May to 31 August 2022. Through sponsorship by South Korea's NIER, these campaigns in which the University of Bremen institute of environmental physics (IUP) DOAS group took part, applied different observation technique such as ground, aircraft, satellite, and model observations to investigate factors responsible for air quality in the Seoul Metropolitan Area, Ulsan, and Busan. On the roof top of the NIER building in Incheon, the IUP MAX-DOAS instrument was mounted and a Pandora instrument part of PGN, sited at Yonsei University Seoul, South Korea.

4.2.1 Co-location of Satellite and Ground-based instrument data product

In this study, the GEMS IUP, GEMS operational and TROPOMI observation products over Incheon and Seoul were co-located with measurements from the MAX-DOAS in Incheon and the Pandora in Seoul. The time span of interest was from October 2021 to November 2022.

Data Collection Method

Key parameters such as timestamps, NO_2 vertical columns, and geographical coordinates (latitude and longitude) were extracted from the datasets. Given the focus on Seoul, timestamps were converted to Korean Standard Time (KST, UTC+9) in other to keep analysis data in local time.

Distance Calculation for Co-location

The co-location process utilized the haversine distance function to calculate the geographic distance of each satellite data point from the MAX-DOAS in Incheon and Pandora in Seoul. This method enabled to determine the proximity of GEMS IUP, GEMS operational and TROPOMI data observation to these fixed MAX-DOAS and Pandora measurements.

Filtering Process for Data Co-location

The GEMS IUP, GEMS operational and TROPOMI data were filtered to retain only those observations within a 5km, 10km and 15 km radius of the MAX-DOAS location in Incheon and Pandora location in Seoul. The GEMS IUP, GEMS operational and TROPOMI data within 15km radius were then used for validation since the results from the different observation radius were comparable to each other. This selective process ensured that the GEMS IUP, GEMS operational and TROPOMI data were geographically relevant to the MAX-DOAS and Pandora measurements. The filtering yielded two distinct subsets of GEMS IUP, GEMS operational and TROPOMI data – one for Incheon and the other in Seoul. These data subsets were then used for further analyses in the study.

Chapter 5

Results and Discussions

5.1.1 Ground and Satellite based Tropospheric NO_2 vertical columns

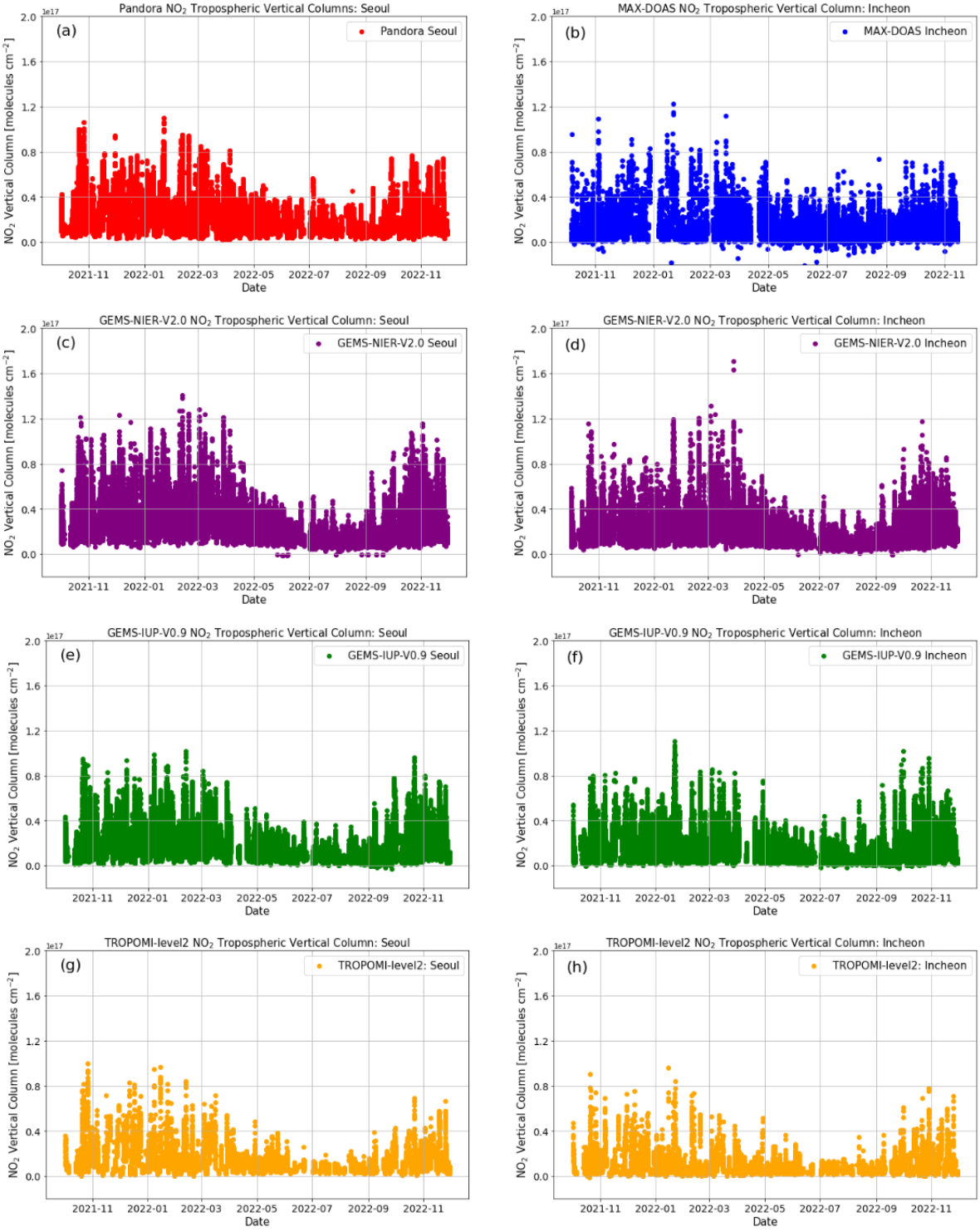

Figure 5.1.1. Tropospheric NO_2 vertical column (10^{17} molecules cm^{-2}) plot of the various instrument products from; (a) Pandora in Seoul, (b) MAX-DOAS in Incheon, (c) GEMS operational product in Seoul, (d) GEMS

operational product in Incheon, (e) GEMS IUP product in Seoul, (f) GEMS IUP product in Incheon, (g) TROPOMI product in Seoul, (h) TROPOMI product in Incheon.

Figure 5.1.1 (a), (b), (c), (d), (e), (f), (g), (h) shows the plot of tropospheric NO_2 vertical columns of Pandora in Seoul, MAX-DOAS in Incheon, GEMS operational product in Seoul, GEMS operational product in Incheon, GEMS IUP product in Seoul, GEMS IUP product in Incheon, TROPOMI product in Seoul, TROPOMI product in Incheon respectively.

The study period spans from October 2021 to November 2022, the data in Figure 5.1.1 (a), (b), (c), (d), (e), (f), (g), (h) shows different seasonal cycles, including parts of two winters, autumns, and one full summer and spring. This period presents the complete spectrum of seasonal variations on tropospheric NO_2 vertical column densities in Seoul and Incheon. The data is from Pandora, MAX-DOAS, GEMS operational and GEMS IUP, and TROPOMI in red, blue, purple, green, and orange colours respectively. Figure 5.1.1 (a), (b), (c), (d), (e), (f), (g), (h) show seasonal variations, with high NO_2 values in colder months, arguably due to longer lifetime and increased heating emissions and lower values in warmer months presumably due to more rapid removal and increased photolysis.

Higher NO_2 levels were observed in the colder months, which span from late October to early March. The observed high values can be attributed to increased emissions from heating due to the cold weather. Lower temperatures also slow down the atmospheric chemical reaction that normally leads to loss of NO_2. Additionally, winter conditions can result in more stable atmospheric layers, leading to less vertical mixing and the accumulation of pollutants closer to the ground in both Seoul and Incheon, accompanied by local variations due to differences in urban heating and industrial activities. Whereas, for the summer months spanning from May to early September, lower NO_2 levels were observed. The reduction in NO_2 is expected due to the increased photolysis rates under longer periods of sunlight, which rapidly break down NO_2. The summer monsoon brings heavy rainfall, which also remove NO_2 from the atmosphere through wet deposition. The frequent cloud cover during this season lead to GEMS (operational and IUP) and TROPOMI reduced sensitivity to ground-level NO_2, potentially contributing to lower observed values. Seoul being more densely populated and urbanised than Incheon which has significant industrial activity, shows different patterns of high and low values. For example, high emissions from traffic and domestic heating in Seoul could have potentially led to consistently higher NO_2 levels compared to Incheon, where industrial emissions and port activities could contribute to NO_2 variability. Seoul is bordered

by 8 mountains (Wikipedia), experiencing high levels of trapped pollutants around the city. Meanwhile, Incheon's coastal location enhances the dispersion of pollutants due to sea breezes; these are reasons why there are differences in NO_2 levels in Seoul and Incheon.

The high and low values of NO_2 observed in Figure 5.1.1 (a), (b), (c), (d), (e), (f), (g), (h) could also be associated with the emission levels from various anthropogenic activities. One of the major human sources of NO_2 is vehicular emissions. Seoul, with dense traffic is associated with higher NO_2 levels, especially during peak rush hours. Incheon on the other hand, with its major port, might experience high NO_2 levels due to emissions from ships and related port activities. Industrial activities are another major contributor to NO_2 emissions. Incheon's industrial zones, including petrochemical complexes and manufacturing plants, could result in higher emission levels, influencing the variability in NO_2 concentrations. During the colder months, the combustion of fossil fuels for residential heating contributes to increased NO_2 levels. This is evident in the winter data for both Seoul and Incheon showing higher values. Also, the demand for power fluctuates with the seasons, affecting NO_2 levels. Other sources such as construction, waste management, and agricultural practices can also contribute to NO_2 emissions, although to a lesser extent compared to transportation and industrial activities.

In addition, the photolysis rate of NO_2 is a crucial factor determining its concentration in the atmosphere. Higher photolysis rates during summer with longer daylight hours and more intense solar radiation result in lower NO_2 concentrations due to faster breakdown. During summer, the extended daylight and higher solar elevation angles increase the photolysis rate. In contrast, during winter, shorter daylight hours and lower solar angles decrease the photolysis rate, contributing to higher NO_2 levels. Cloud cover, which can be more prevalent during the monsoon season, can reduce the effective solar radiation reaching the NO_2 molecules, thereby decreasing the photolysis rate while clear skies on sunny days enhance the photolysis rate.

Some of the factors responsible for the tropospheric NO_2 transport, which involves the movement and dispersion of NO_2 in the atmosphere, are wind and atmospheric stability. Wind can transport NO_2 away from its source causing a decrease in local concentrations and an increase in downwind area like Seoul. The variability in wind speed and direction can lead to day-to-day fluctuations in NO_2 levels as observed in Figure 5.1.1 (a), (b), (c), (d), (e), (f), (g), (h). Another factor which is the stability of the atmosphere affects vertical mixing. During stable conditions, often occurring in the winter, there is less vertical mixing, which can trap

NO_2 close to the ground, leading to higher concentrations as we could see in the different figures. While on the other hand, an unstable condition often in the warmer months enhances the dispersion and dilution of NO_2. For example, frequent winds in circulation during winter from industrial areas towards residential areas could as well transport $NO_2$from one region to another resulting to higher NO_2 measurement in the residential areas. But then, strong winds during the summer monsoon could have dispersed NO_2 more effectively resulting to lower overall concentrations.

From Figure 5.1.1 (a), (b), (c), (d), (e), (f), (g), (h), we also try to show the influence of energy usage on NO_2 levels in Seoul and Incheon. In winter months, there is an increased demand for heating in residential and commercial buildings. This often leads to higher emissions of NO_2, especially if the energy is generated from the combustion of fossil fuels like coal, oil, or natural gas. Thus, higher NO_2 levels in winter months can partly be attributed to increased energy usage for heating. Industrial activities and power generation are another major source of NO_2 emissions, in the sense that any fluctuations in industrial production or changes in the energy production source can alter NO_2 levels especially in Incheon that have heavy industries.

5.2.1 Hourly variations

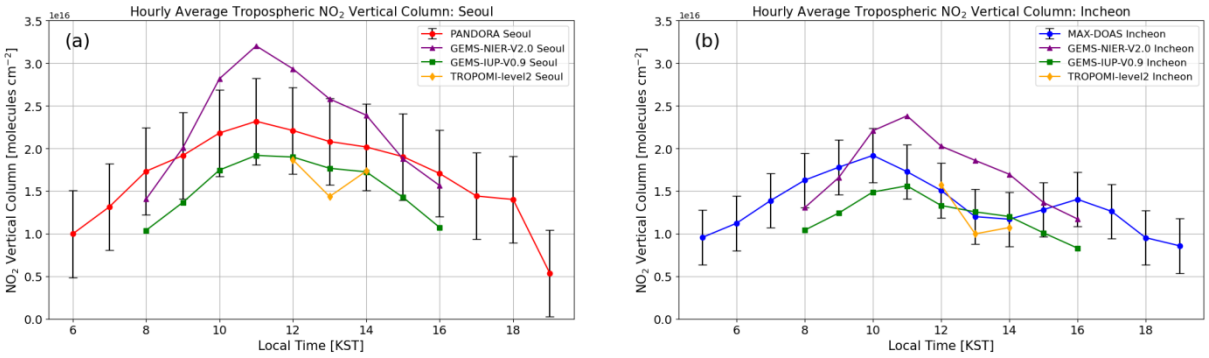

Figure 5.2.1 Hourly average variation of tropospheric NO_2 vertical column (10^{16} molecules cm^{-2}) in (a) Seoul and (b) Incheon. Different colours indicate different datasets. All data from October 2021 to November 2022 have been averaged. The error bars in the figures represent the standard deviation of the measured tropospheric NO_2 vertical columns, providing an indication of the variability in the data throughout each hour over the averaging period.

Figure 5.2.1 show the hourly average tropospheric NO_2 vertical column (10^{16} molecules cm^{-2}) variation in (a) Seoul and (b) Incheon. Different colours indicate different datasets. All data from October 2021 to November 2022 were averaged.

Figure 5.2.1 (a): Hourly variation in Seoul

At 6:00, the Pandora instrument measurement have a value of 1.00 x 10^{16} molecules cm^{-2}, it then peaks at approximately 2.32x10^{16} molecules cm^{-2} between 10:00 and 12:00, and then gradually decreases back to around 0.53x10^{16} molecules cm^{-2} by 19:00. The GEMS operational product begins at around 1.40x10^{16} molecules cm^{-2} at 8:00, and reaches a peak value at nearly 3.20x10^{16} molecules cm^{-2} around 11:00, and decreases to about 1.56x10^{16} molecules cm^{-2} by 16:00. While, the GEMS IUP measurements start at about 1.04x10^{16} molecules cm^{-2} at 8:00, and peak at around 1.92x10^{16} molecules cm^{-2} between 11:00 and noon, it reaches its minimum value of 1.07x10^{16} molecules cm^{-2} by 16:00. The TROPOMI measurements show a peak value of 1.87 x 10^{16} molecules cm^{-2} at noon, minimum value of 1.43x 10^{16} molecules cm^{-2} at 13.00 and a value of 1.73x 10^{16} molecules cm^{-2} at 14:00. There is a good agreement between the Pandora and the GEMS IUP dataset compared to the agreement between the Pandora and GEMS operational product. The GEMS operational product show much more scatter.

Figure 5.2.1 (b): Hourly variation in Incheon

The MAX-DOAS measurement starts at about 0.96x10^{16} molecules cm^{-2} at 5:00, peaks at around 1.92x10^{16} molecules cm^{-2} at 10:00, then decreases to 1.20x10^{16} molecules cm^{-2} between 13:00 and 14:00 and peaks again at around 1.40x10^{16} molecules cm^{-2} at 16:00, then finally falls to around 0.86x10^{16} molecules cm^{-2} by 19:00. The GEMS operational product begins at approximately 1.30x10^{16} molecules cm^{-2} at 8:00, and peaks at 2.38x10^{16} molecules cm^{-2} around 11.00, then drops to about 1.17x10^{16} molecules cm^{-2} by 16:00. The GEMS IUP show a start at around 1.04x10^{16} molecules cm^{-2} at 8:00, peaks at about 1.56x10^{16} molecules cm^{-2} at 11:00, and then decreases to around 0.83x10^{16} molecules cm^{-2} by 16:00. The TROPOMI measurements show a peak value of 1.57 x 10^{16} molecules cm^{-2} at noon, and a minimum value of 1.00x 10^{16} molecules cm^{-2} at 13:00 and a value of 1.07x 10^{16} molecules cm^{-2} at 14:00. There is a better agreement between the MAX-DOAS and the GEMS IUP compared to the agreement between the MAX-DOAS and GEMS operational product.

Difference between instrument measurements in Seoul and Incheon

Figure 5.2.1 show that peak tropospheric NO_2 levels in Seoul are higher than those in Incheon, with the GEMS operational product measuring the larger peaks. In contrast, the NO_2 levels in Incheon, particularly those measured by the MAX-DOAS, show a distinct double-peak pattern within the daily cycle, a pattern which is not clearly observed in the Seoul

measurements. The variability in NO_2 levels throughout the day is higher in Seoul compared to Incheon, as shown by the wider range of values. The TROPOMI values are lower than those of GEMS product and the ground based measurement values. The GEMS IUP follows similar pattern of Pandora and MAX-DOAS hourly peak and trough pattern at similar time of day which shows a good agreement. Additionally, the GEMS operational product has a tendency to overestimate higher ground-based measurement values and underestimate the lower ground based values. Conversely, the GEMS IUP values consistently underestimate the ground based measurement values at all times. Another feature is that the MAX-DOAS instrument start measuring earlier at 5:00 and stop at 19:00, while the Pandora instrument start at 6:00 and stop at 19:00 than the GEMS product that start taking measurement at 8:00 and stop at 16:00. In addition, the TROPOMI data agrees better with the GEMS IUP product. This observation iterates the point that TROPOMI's measurements are more closely aligned with GEMS IUP than with other datasets, as observed in both Incheon and Seoul. However, the TROPOMI do not show as much consistency with the operational product or the Pandora measurements in Seoul but they agree quite well with both GEMS IUP and MAX-DOAS products in Incheon. The lower TROPOMI values are partly due to the timing of TROPOMI measurements around midday, unlike GEMS, which measures NO_2 throughout the entire day. In the diurnal cycle, NO_2 values at noon are higher than those in the early morning and evening, TROPOMI's values would be lower than GEMS full-day values because TROPOMI measures in the afternoon. Additionally, the differences in the datasets can be attributed to the distinct assumptions applied during the retrieval of the tropospheric NO_2 vertical column. With the GEMS instrument, for the first time from space, NO_2 diurnal variation can be measured by a satellite instrument. This capability differentiates the GEMS instrument from other instrument as the first satellite instrument capable of providing several NO_2 measurements per day from geostationary earth orbit. Within comparison, the TROPOMI instrument, a low earth sun synchronous orbit instrument has just one measurement per day, the time of observation varying by +/- one hour.

Impact of emissions

Traffic patterns have a pronounced effect on the diurnal variation of NO_2 levels due to the emissions from vehicles. Before the morning rush hour, NO_2 levels may start at a baseline that reflects overnight conditions. As traffic begins to increase with people starting their daily commutes, NO_2 levels rise. However, the morning rush hour period result to noticeable spike in NO_2 levels as vehicle emissions increase. The morning peak in NO_2 levels corresponds

with the highest traffic volume of the day. Also, Figure 5.2.1 shows that the NO_2 levels dips after the morning rush as traffic decreases before observing another slight increase in NO_2 levels in the evening when people travel from work, though this peak is usually lower than in the morning. But as vehicular traffic reduces further into the night, NO_2 levels decreases. However, the rate of decrease can be influenced by factors such as remaining traffic, the dispersion of NO_2 in the atmosphere, and the reduction of photolytic activity after sunset. Daily rush hours also increases vehicular traffic as people commute to and from work, school, and other daily activities. This influx of vehicles is a primary source of NOx, including NO_2. During the morning rush hour, which spans from 6:00 to 11:00, NO_2 levels are expected to rise as a large number of vehicles are on the roads, emitting pollutants from their exhausts. This peak in NO_2 is often the most pronounced of the day due to the combination of increasing traffic and stable atmospheric conditions that trap pollutants near the ground. Another rush hour which is the evening rush hour, usually from 15:00 to 19:00, can also lead to increased NO_2 levels. However, the evening peak may not be as high as the morning peak for several reasons. Photolysis has been occurring throughout the day, reducing the overall levels of NO_2. Additionally, the dispersal of the evening commute over a longer period or the less synchronous nature of evening activities compared to the morning rush can lead to a broader, less pronounced peak.

Impact of photochemistry

The rate of photolysis is dependent on the intensity of sunlight, which varies throughout the day. At sunrise, as the intensity of sunlight increases, the rate of photolysis increases, leading to a decrease in NO_2 levels. The highest photolysis rates occur around noon when solar radiation is at its peak, often corresponding to the lowest daily NO_2 levels. The effect of photolysis on NO_2 levels is evident in the midday dip observed in Figure 5.2.1 (a), (b). After the morning traffic rush hour, the increased photolysis rates contribute to the decrease in NO_2 column amount. The combined effects of traffic patterns and photolysis result in characteristic diurnal NO_2 patterns. Morning peaks due to traffic emissions are followed by decreases as photolysis rates increase, with smaller peaks in the evening as photolysis decreases and traffic emissions continue.

Solar radiation significantly influences the diurnal variation of NO_2 concentrations due to its role in the photolytic breakdown of NO_2. This can be seen in Figure 5.2.1, which shows the hourly average tropospheric NO_2 vertical column in Seoul (a) and Incheon (b). In the morning, solar radiation begins to increase but is not yet at its peak, so the photolysis of NO_2

is relatively low enabling the NO_2 concentrations to increase due to morning traffic emissions. But as the sun reaches its zenith, solar radiation is at its strongest, leading to the highest photolysis rates of the day at midday. This results in a decrease in NO_2 levels as it is broken down into nitrogen oxide (NO) and ozone (O_2). Into the afternoon, solar radiation starts to decrease; the photolysis rate is still significant enough to maintain lower levels of NO_2 compared to the morning. As the sun sets, solar radiation diminishes, reducing the photolysis rate. The lack of photolytic activity during the evening and night allows NO_2 concentrations to remain or increase slightly, especially if there is evening rush hour traffic. This evening variation is shown by the different instrument products but more clearly shown by the MAX-DOAS in Incheon.

Impact of meteorology

In Figure 5.2.1 (a), (b), the effects of atmospheric stability can be seen in the patterns of NO_2 concentration. Higher levels of NO_2 in the early morning correlate with a more stable atmosphere, while lower concentrations during the day are associated with increased atmospheric instability. The stability of the atmospheric layer influences the concentration and dispersion of NO_2. This stability is determined by change in atmospheric condition, which affects the vertical movement of air as well as NO_2. During stable atmospheric conditions, which occur during the night and early morning, the air near the surface is cooler than the air above. This temperature inversion prevents vertical mixing, trapping pollutants like NO_2 close to the ground and leading to higher concentrations. Meanwhile, during the day, the ground heats up due to solar radiation, causing the air near the surface to become warmer than the air above. This situation leads to an unstable atmosphere where warmer, less dense air rises, allowing for vertical mixing and dispersion of pollutants, resulting in lower concentrations of NO_2 at ground level.

The depth of the atmospheric boundary layer varies; it is shallower in the morning and expanding in the afternoon. Due to these differences, column measurements disagree with in-situ measurement reporting NO_2 concentrations at the surface. For air quality measurement, ground-level pollution is of utmost relevance due to its direct health implications, and satellite data, which are not ground based, cannot be applied directly to health impact studies because it would be misleading depending on the thickness of the atmospheric boundary layer. Moreover, satellite measurements are less reliable during times when the sun is low in the sky, as in the mornings and evenings, due to the lower levels of sunlight. The dataset, averaged over a year, has inherent biases, such as the absence of morning and evening

measurements during winter. Consequently, the diurnal variation depicted in Figure 5.2.1 is to some extent biased because the morning and evening values are acquired solely from summer data, while the noon values are collected year-round. If we consider seasonality effects, such as lower NO_2 levels in summer, then the plotted full-year diurnal variation could present a bias, appearing in the mid-range. For instance, if NO_2 levels are higher in winter and lower in summer, values at noon will be averaged and in the middle of the two datasets, while values in the morning and evening are only from summer and therefore lower, the lower morning and evening values therefore do not necessarily imply that NO_2 values are low in the morning, they could also be the result of NO_2 values being lower in summer.

5.3.1 Seasonal variations

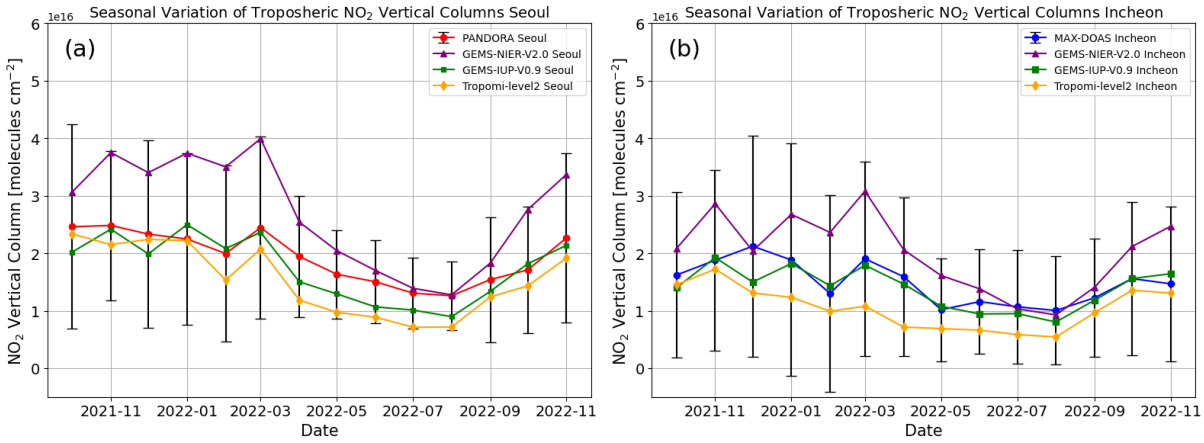

Figure 5.3.1 Seasonal variation (monthly averages) of tropospheric NO_2 vertical column (10^{16} molecules cm^{-2}) in (a) Seoul and (b) Incheon. Measurements at all times of the day are averaged.

Figure 5.3.1 show the seasonal variation of tropospheric NO_2 vertical column (10^{16} molecules cm^{-2}) in Seoul and Incheon, based on monthly averages from October 2021 to November 2022.

Figure 5.3.1 (b): Seasonal variation in Seoul

The Pandora data show a seasonal variation with peaks between November 2021 to March 2022 then another peak in November 2022, with the highest peak value of $2.44x10^{16}$ molecules cm^{-2}. The lowest values are observed around July and August 2022 measuring $1.31x10^{16}$ molecules cm^{-2}. The GEMS operational product shows a similar pattern with higher peaks and trough. The highest peak value measured is $3.99x10^{16}$ molecules cm^{-2}, and the lowest value is around $1.27x10^{16}$ molecules cm^{-2} in August 2022. The GEMS IUP values also follow a similar seasonal pattern but with lower peaks, around $2.50x10^{16}$ molecules cm^{-2} in

January 2022, and trough approximately $0.90x10^{16}$ molecules cm^{-2} in August 2022. The TROPOMI shows much lower variations compared to other instruments, with a range between $2.33x10^{16}$ molecules cm^{-2} in October 2021 and $0.72x10^{16}$ molecules cm^{-2} in August 2022. All the instruments appear to follow a similar seasonal variability with variations in magnitude. This shows a good agreement on the seasonal pattern of NO_2 levels. During the colder months, the GEMS operational product shows a distinct peak that is not as pronounced in the other products. The GEMS operational product value is around 38% overestimating the Pandora values in magnitude. However, the GEMS IUP values underestimate the Pandora values by approximately 12%. The GEMS IUP product shows good agreement when compared with the Pandora values.

Figure 5.3.1 (b): Seasonal variation in Incheon

The MAX-DOAS presents peaks in December 2021, March 2022 and a lower peak in October 2022, with December 2021 peak reaching a maximum value of 2.12×10^{16} molecules cm^{-2}. The lowest values are around 1.00×10^{16} molecules cm^{-2}, observed in May, July and August 2022. The GEMS operational product shows similar seasonal pattern like in Seoul but with a lower magnitude. The maximum peak is in March 2022 at 3.08×10^{16} molecules cm^{-2} and the lowest value at $0.93x10^{16}$ molecules cm^{-2} in August 2022. The GEMS IUP data shows a maximum peak value of $1.92x10^{16}$ molecules cm^{-2} in November 2021 and have a minimum value of $0.80x10^{16}$ molecules cm^{-2} in August 2022. The TROPOMI Indicates a slight peak value of $1.72x10^{16}$ molecules cm^{-2} in November 2022, with the lowest values reaching $0.55x10^{16}$ molecules cm^{-2} during the summer months. The MAX-DOAS, the GEMS operational product, and the GEMS IUP data sets show closer variation across the year, although the GEMS operational product still overestimates the MAX-DOAS values by 44%. However, the GEMS IUP data underestimates the MAX-DOAS value by 7%. Hence, The MAX-DOAS agrees much better with the GEMS IUP product which is a good indication of consistent measurements between these instruments.

The TROPOMI data in both Seoul and Incheon follows the same seasonal variation but with lower values, this could be due to its overpass time, which measures NO_2 levels when they are relatively low, as seen in Figure 5.2.1. Both cities exhibit higher NO_2 levels during the colder months (late fall, winter, early spring). This could be due to increased heating and energy use in the colder months, more stable atmospheric conditions that limit dispersion patterns of NO_2, lower solar radiation resulting to slow photochemistry taking place in the atmosphere. In both cities, summer months show the lowest NO_2 columns, which could be associated with

lower emissions due to less heating activity, cloud cover and high precipitation removing NO_2 from the atmosphere.

5.4.1 Tropospheric NO_2 vertical column weekly cycle

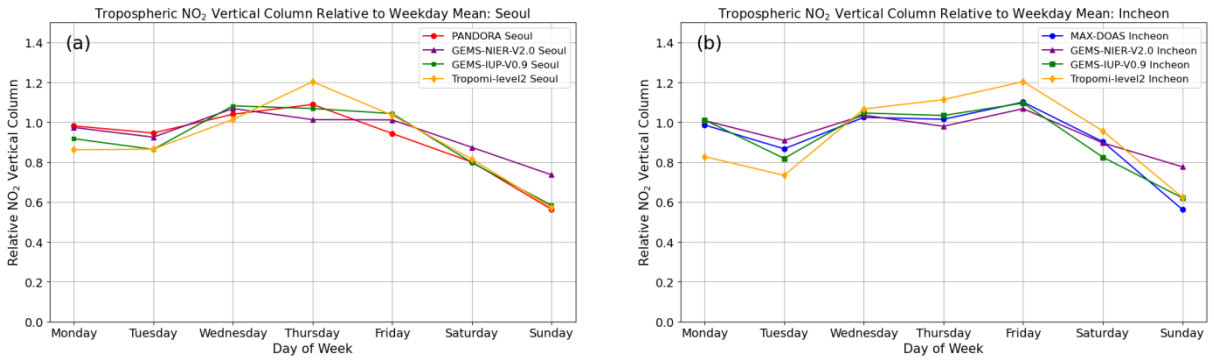

Figure 5.4.1a. Mean weekly variation of relative (averages over daily values divided by the mean over the weekdays; unit-less values) tropospheric NO_2 vertical column for (a) Seoul and (b) Incheon without the TROPOMI

Figure 5.4.1 (a), and (b) show the mean weekly variation of relative tropospheric NO_2 vertical column in Seoul and Incheon averaged over daily values divided by the mean over the weekdays; (unit-less values). The relative values were derived by dividing daily values by the mean over working days (Mondays – Fridays)

The relative NO_2 levels in Seoul are consistent across the weekdays and start to show a downward trend as the weekend approaches with the lowest levels on Sunday. Similar to Seoul, the measurement in Incheon show a good agreement on the pattern of NO_2 levels throughout the week, with the GEMS operational product following the same general trend with slight deviations on Sunday and TROPOMI value been lowest on Monday. There is a noticeable decrease in the NO_2 levels towards the weekend, again lowest on Sunday, reflecting a likely reduction in pollution due to reduced weekend activities. In Figure 5.4.1 (b), the measurement in Incheon shows a bit more variability in the relative NO_2 levels between the instruments compared to Seoul, but the general pattern of a decrease towards the weekend remains clear.

In Seoul, Figure 5.4.1 (a), the Friday, Saturday and Sunday relative NO_2 levels for Pandora, GEMS operational, GEMS IUP and TROPOMI were (0.94, 1.01, 1.04, 1.03), (0.80, 0.87, 0.77, 0.81) and (0.56, 0.74, 0.58, 0.57) respectively. Meanwhile, in Figure 5.4.1 (b), Incheon, the Friday, Saturday and Sunday relative NO_2 levels for MAX-DOAS, GEMS operational,

GEMS IUP and TROPOMI were (1.10, 1.07, 1.09, 1.20), (0.90, 0.90, 0.83, 0.96) and (0.56, 0.78, 0.62, 0.62) respectively which also shows around 20% reduction on Saturday and 40% reduction on Sundays in both cities. Based on these results, we could infer that the GEMS IUP agree reasonably better when compared with Pandora and MAX-DOAS than GEMS operational compared with Pandora and MAX-DOAS, then TROPOMI possess the lowest Sunday minimum value followed by GEMS IUP in both Seoul and Incheon.

In research conducted by Stavrakou et al., (2020), the variation in weekly NO_2 levels was examined across multiple urban areas utilizing data from the annually averaged OMI and TROPOMI products. For OMI (2005 to 2017), the weekly cycle NO_2 values for Friday, Saturday, and Sunday in Seoul and Busan showed a ratio of (0.99, 0.86 (percentage reduction = 13), 0.88 (11)) and (1.00, 0.93(7), 0.80(20)) respectively. For TROPOMI, which spanned from May 2018 to April 2019, the weekly cycle of NO_2 values for Friday, Saturday, and Sunday in Seoul and Busan showed a ratio of (1.22, 1.04 (15), 0.72 (41)) and (1.10, 0.93(15), 0.78(29)) respectively. Upon comparison with the weekly cycle result of this study, it is evident that in Seoul, there have been significant reductions in NO_2 weekly levels over time, which is most likely the case in Incheon and other cities in South Korea, as a result of the pollution control policies by South Korea (Seo et al., 2021).

5.4.2 Monthly weekend to weekday effect

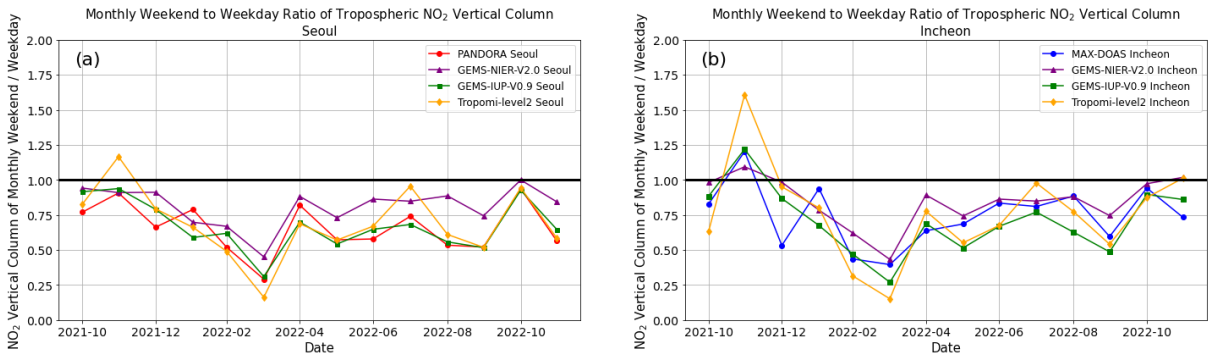

Figure 5.4.2. Monthly effects plots of weekend to weekday ratio, (averages over monthly weekend values divided by mean monthly weekday values; unit-less values) of tropospheric NO_2 vertical column in; (a) Seoul, and (b) Incheon.

Figure 5.4.2 (a), and (b) show the mean monthly variation of relative tropospheric NO_2 vertical column in Seoul and Incheon averaged over monthly values divided by the mean monthly weekdays; (unit-less values). The observation in Seoul shows relative consistency in the weekend to weekday NO_2 ratio over time, with small variations implying that of NO_2

emissions on weekends versus weekdays does not undergo large changes throughout the period of study.

Between February and April the ratio dips lowest below the horizontal 1 line, suggesting that on these weekends, NO_2 levels were much lower than the weekday average compared to other months showing a constant pattern below the horizontal 1 line. We see the TROPOMI value slightly exceeds the horizontal 1 line in November for Seoul. We can infer that the relatively smooth pattern over time shows that the factors influencing NO_2 emissions, such as traffic volume and industrial activity, remain constant from month to month over the season. In Incheon, the variability in the ratio seems more noticeable, with sharper peaks above the horizontal 1 line in November 2021 and lowest troughs in March 2022 by all instrument observation, and showing noticeable changes from month to month then varying below the horizontal 1 line implies also that the NO_2 levels on weekends are comparable to weekdays. The absence of a strong seasonal variation in both Seoul and Incheon suggests that, the anthropogenic sources of NO_2 emissions are constant with the seasons.

5.4.3 Weekly weekend to weekday effect

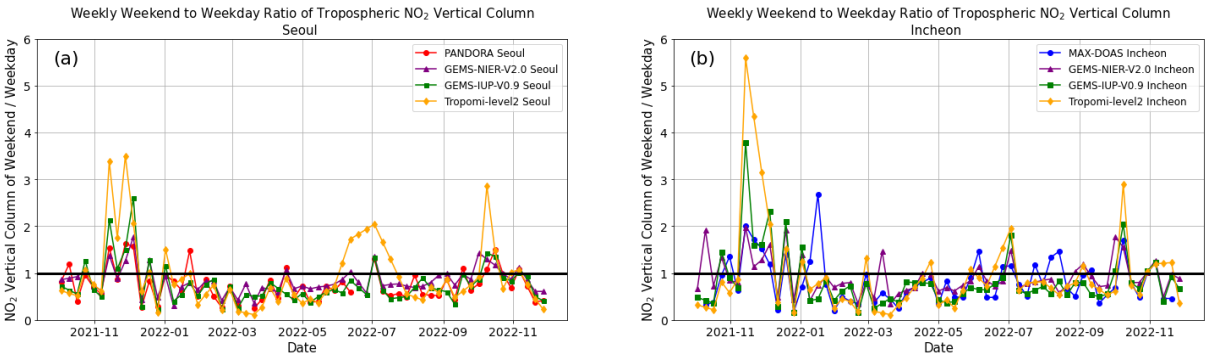

Figure 5.4.3. Weekly effects plots of weekend to weekday ratio, (averages over weekly weekend values divided by mean weekly weekday values; unit-less values) of tropospheric NO_2 vertical column in (a) Seoul, and (b) Incheon.

Figure 5.4.3 (a), and (b) show the mean weekly weekend to weekday ratio of tropospheric NO_2 vertical column in Seoul and Incheon averaged over weekly weekend values divided by the mean weekly weekday value; (unit-less values).

In this figure, we observe considerable variability, suggesting that each week might present slightly different conditions. However, when comparing the various lines, they often exhibit the same pattern. The depicted peaks and dips are consistently mirrored across the different time series, indicating atmospheric changes. A monthly average would smooth out some of

this week-to-week variability, providing a more distinct view of the changes over time. In November 2021, there is a notable anomaly, which is as a result of few data caused by poor weather conditions. The first implication is that there seems to be good agreement in different measurements particularly regarding the weekly variations observed within individual weeks, despite the variability that all instruments measures. TROPOMI shows the most pronounced peaks, which could be attributed to its smaller dataset size (one measurement per day instead of several hourly measurements as for GEMS and the ground-based instruments).

The variability could be influenced by factors like cloud cover in Incheon compared to Seoul or vice versa, or wind patterns that may carry pollution towards one of the locations. Identifying specific causes can be challenging as such variability is often just statistical and related to weather conditions since pollution levels are influenced by factors like wind speed and direction, precipitation, cloud cover, temperature, and emissions. This atmospheric variability makes identifying the exact relationship between pollution levels and emissions difficult for a single measurement. Nonetheless, on average, emissions remain constant, and the weather related variability tends to balance out over time that is why we used a full year of data in other analysis to obtain a reliable average. When looking at the yearly data, showing the weekly effect in Figure 5.4.3 for the full time series we could see more of the atmospheric noise due to the impact of meteorology and also chemistry as well as rainfall but less in the monthly effect in Figure 5.4.2

The conclusions drawn from Figure 5.4.3 is that the instruments measures very similar patterns. They show that the weekly seasonal cycle varies, with lower NO_2 levels on weekdays and even lower on weekends. Atmospheric variability has a significant impact on air pollution levels, but the data also show that most data points fall below the ratio 1 horizontal line, indicating less pollution on weekends compared to weekdays. However, during periods where peaks exceed the ratio of 1, the NO_2 levels are higher on weekends. This implies that while pollution is lower on weekends, this is not a consistent pattern every week.

Chapter 6

Validation results

6.1.1 Hourly comparison of Ground-based and satellite observation

Figure 6.1.1 shows hourly comparison of tropospheric NO_2 vertical column; (a) Pandora and GEMS operational product in Seoul, (b) Pandora and GEMS IUP product in Seoul, (c) MAX-DOAS and GEMS operational product in Incheon, (d) MAX-DOAS and GEMS IUP product in Incheon (e) Pandora and TROPOMI product in Seoul and (f) MAX-DOAS and TROPOMI product in Incheon. GEMS like every other satellite instrument averages over large areas, whereas MAX-DOAS provides localized averages along its line of sight, which result in a relatively smaller air volume probe compared to the satellite.

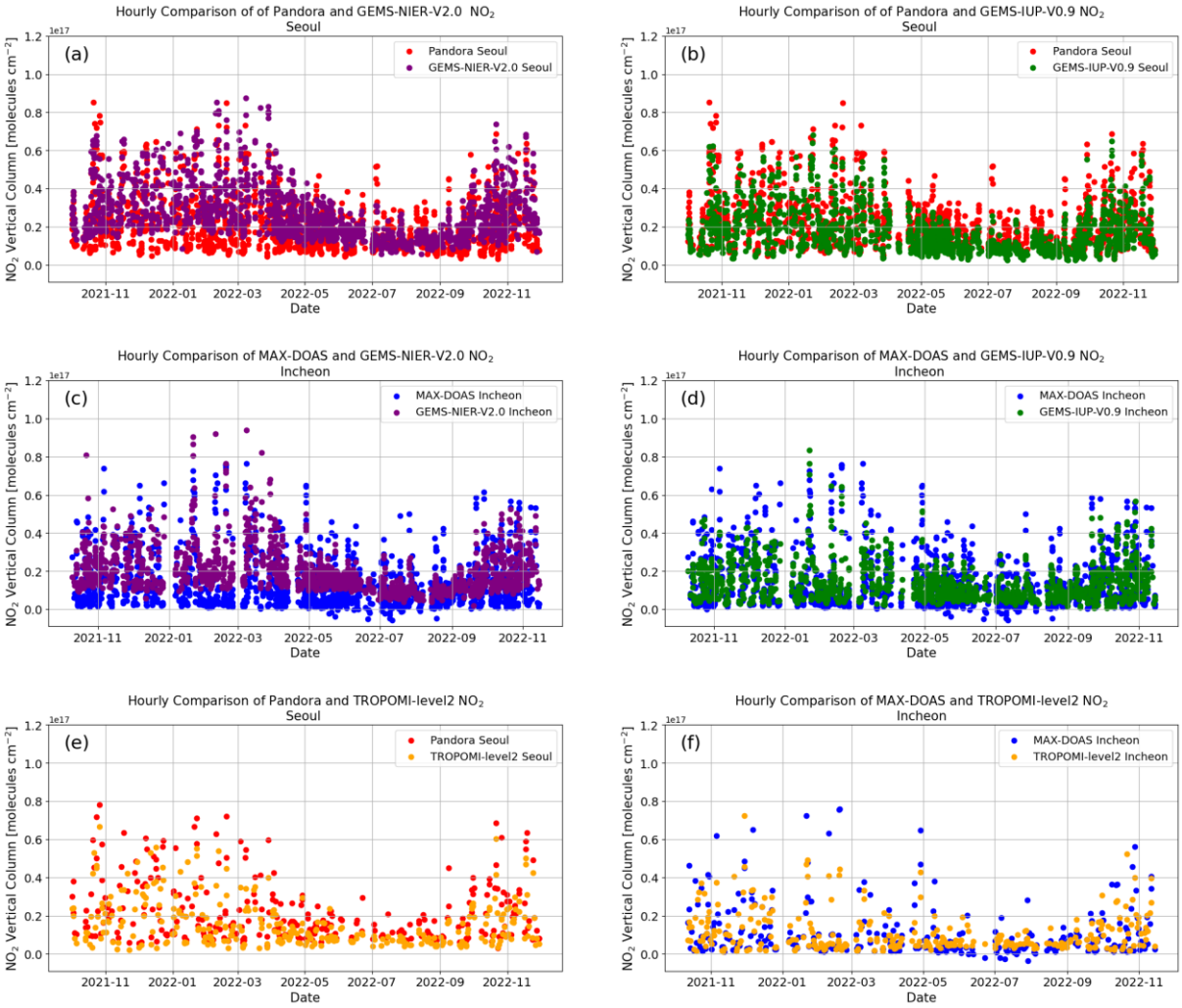

Figure 6.1.1 Hourly comparison plot of tropospheric NO_2 vertical column (10^{17} molecules cm^{-2}) from; (a) Pandora and GEMS operational product in Seoul, (b) Pandora and GEMS IUP product in Seoul, (c) MAX-DOAS and GEMS operational product in Incheon, (d) MAX-DOAS and GEMS IUP product in Incheon (e) Pandora and TROPOMI product in Seoul and (f) MAX-DOAS and TROPOMI product in Incheon.

Additionally, MAX-DOAS and Pandora instruments observe from the ground, while the GEMS instrument observes from above. This difference implies that ground-based measurements are more sensitive to surface-level NO_2 than GEMS measurements.

Seoul Comparison:

Pandora and GEMS operational product (a): The GEMS operational product often measures higher NO_2 vertical column than the Pandora measurements at the lower vertical scale. Also, there is a large scatter of data points with Pandora measuring higher NO_2 vertical columns than GEMS operational product. This suggests a consistent pattern of overestimation by the Pandora product.

Pandora and GEMS IUP Product (b): Displays a tighter cluster of data points with less variability between the Pandora and GEMS IUP measurements, indicating a better agreement between the two datasets but also underestimation by the GEMS IUP product.

Pandora and TROPOMI Product (e): Exhibits significant variability with some points indicating that Pandora records much higher vertical columns. This is suggesting an overestimation in comparison to TROPOMI data.

Incheon Comparison:

MAX-DOAS and GEMS Operational Product (c): Shows a broad spread of data points with MAX-DOAS often measuring higher NO_2 levels than GEMS operational product, indicating a tendency for the MAX-DOAS to overestimate relative to GEMS operational data. At the lower vertical scale, the GEMS operational product tends to measure higher NO_2 values than the MAX-DOAS measurements.

MAX-DOAS and GEMS IUP Product (d): These two products have a more consistent alignment between the datasets and with a better agreement between MAX-DOAS and GEMS IUP measurements. The GEMS IUP values underestimate that of the MAX-DOAS measurement.

MAX-DOAS and TROPOMI Product (f): Show a pattern where the MAX-DOAS NO_2 measurements are higher than the TROPOMI measurements, indicating that the TROPOMI values are underestimating the MAX-DOAS values.

Figure 6.1.1 indicates a good general agreement between the ground-based and satellite instruments with underestimation of NO_2 vertical columns by the satellite instruments

compared to the ground-based instruments. In Figure 6.1.1, only the measurements which have matching times are plotted, and therefore, these are much less data points than in previous plots. This is very obvious for the TROPOMI measurement in figure 6.1.1 (e) and (f).

6.2.1 Hourly scatter plot

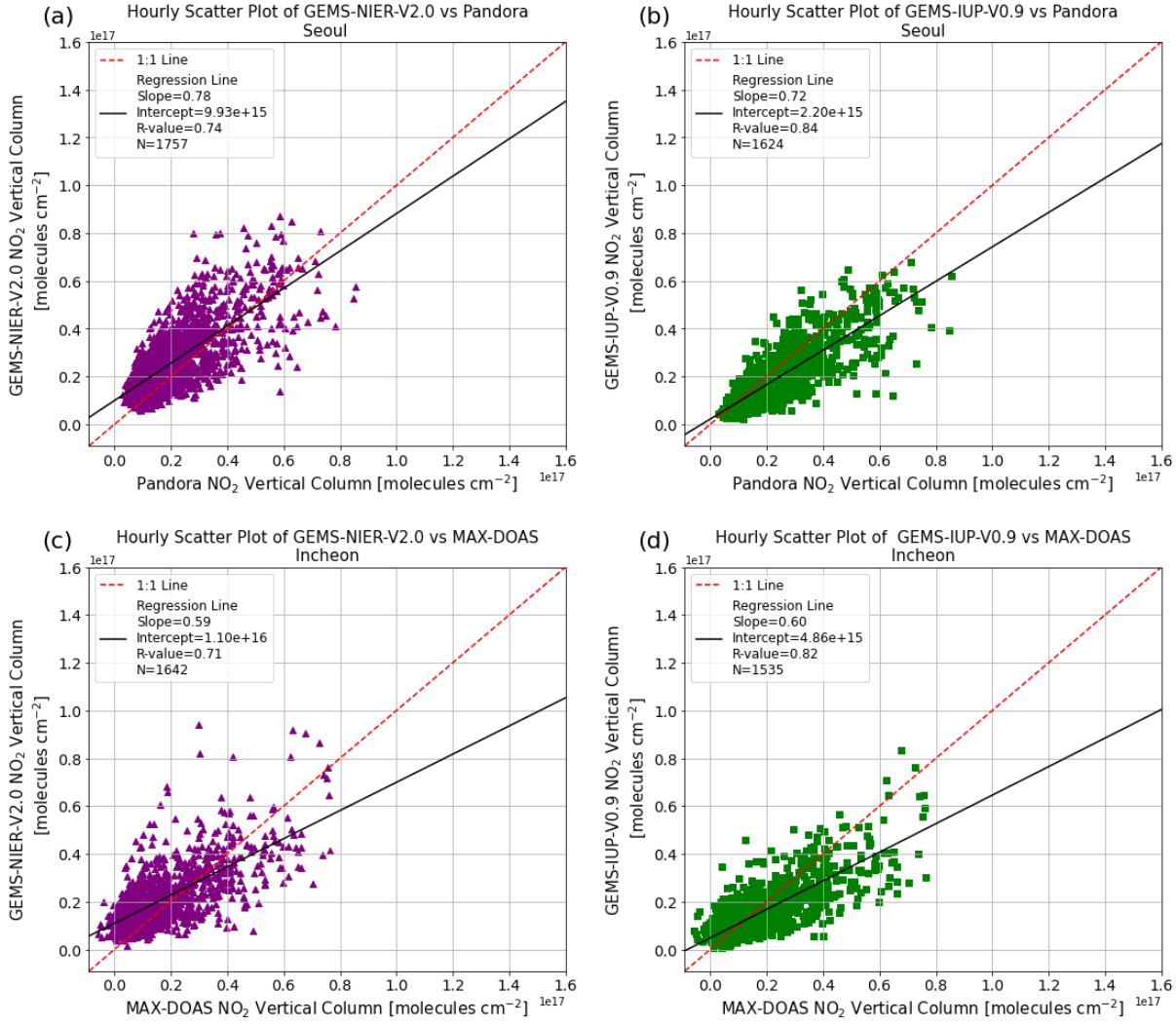

Figure 6.2.1. Scatter plot of hourly tropospheric NO_2 vertical column (10^{17} molecules cm^{-2}) from; (a) GEMS-NIER-V2.0 against Pandora in Seoul, (b) GEMS-IUP-V0.9 against Pandora in Seoul, (c) GEMS-NIER-V2.0 against MAX-DOAS in Incheon, (d) GEMS-IUP-V0.9 against MAX-DOAS in Incheon. In this figure, only daily mean hourly matching values between respective instruments are plotted against each other.

Table 2: Statistical results of the hourly comparisons between the two GEMS products and ground based validation measurements.

Figure	Location	Comparison Instruments	Slope	Intercept ($x10^{16}$ molecules cm^{-2})	R-value	N	Mean Absolute Bias ($x10^{16}$ molecules cm^{-2})	Mean Relative Bias (%)
(a)	Seoul	GEMS operational product vs. Pandora	0.78	0.99	0.74	1757	0.86	34
(b)	Seoul	GEMS IUP product vs. Pandora	0.72	0.22	0.84	1624	0.54	39
(c)	Incheon	GEMS operational product vs. MAX-DOAS	0.59	1.10	0.71	1642	0.90	54
(d)	Incheon	GEMS IUP product vs. MAX-DOAS	0.60	0.49	0.82	1535	0.56	49

The scatter plots in Figure 6.2.1 compare hourly tropospheric NO_2 vertical column measurements between GEMS operational and GEMS IUP product with Pandora in Seoul and MAX-DOAS in Incheon. Each plot shows the relationship between the two sets of measurements, with the statistical results providing insight into their correlation, bias, and the number of matched data points (N).

Comparisons results in Seoul (a and b)

GEMS operational product vs. Pandora: The slope of 0.78 and an R-value of 0.74 shows a good positive correlation, which suggests that GEMS operational product increase alongside with Pandora. However, a slope less than 1 implies that the GEMS operational product underestimates NO_2 compared to Pandora. The intercept of $0.99x10^{16}$ molecules cm^{-2} suggests that when the Pandora value is at zero, then the GEMS operational value would be close to $0.99x10^{16}$ molecules cm^{-2}, Pandora values lower than the GEMS operational product. The mean absolute bias of $0.86x10^{16}$ molecules cm^{-2} and a relative bias of 34% show consistent bias between GEMS operational product and Pandora.

GEMS IUP vs. Pandora: A higher R-value of 0.84 with a slope of 0.72 suggests a slightly stronger positive correlation but also a clear underestimation by the GEMS IUP product. The lower intercept of 0.22 $x10^{16}$ molecules cm^{-2} indicates a smaller difference in values between

GEMS IUP and Pandora at small NO_2 columns than between the GEMS operational product and Pandora. The mean absolute bias is lower at $0.54x10^{16}$ molecules cm^{-2}, but the mean relative bias is higher at 39%. The reason for the larger relative bias is the lower absolute values in the GEMS IUP product.

Comparisons results in Incheon (c and d)

GEMS operational product vs. MAX-DOAS: With a slope of 0.59 and an R-value of 0.71, there is a good correlation, but the large slope deviation from 1 indicates that the GEMS operational product underestimates NO_2 compared to MAX-DOAS. A higher intercept of $1.10x10^{16}$ molecules cm^{-2} shows that the GEMS operational product tends to have high NO_2 values at small columns. The biases are higher with a mean absolute bias of $0.90x10^{16}$ molecules cm^{-2} and a mean relative bias of 54%, suggesting that GEMS operational product underestimates MAX-DOAS.

GEMS IUP vs. MAX-DOAS: The slope of 0.60 and an R-value of 0.82 indicate a strong correlation and similar underestimation as seen with the GEMS operational product. The intercept of $0.49x10^{16}$ molecules cm^{-2} suggests less bias between GEMS IUP and MAX-DOAS compared to plot of GEMS operational product vs. MAX-DOAS. The mean absolute bias and relative bias are slightly lower than for the GEMS operational product vs. MAX-DOAS but still shows underestimation by GEMS IUP.

From the hourly scatter plot, it can be seen that all comparisons show a strong positive correlation between ground-based and satellite measurements, with somewhat better correlations for the GEMS IUP product. However, there is underestimation by the GEMS operational and GEMS IUP product compared to the Pandora and MAX-DOAS measurements, as indicated by the slopes being less than 1 and the biases.

6.3.1 Time of day scatter plot

Figure 6.3.1 shows scatter plots of the time of day mean tropospheric NO_2 vertical column for (GEMS operational and GEMS IUP) product vs. Pandora and MAX-DOAS comparisons in Seoul and Incheon.

Comparisons results in Seoul (a and b)

(a) GEMS operational product vs. Pandora: A very high R-value (0.99) and a slope (3.01) greater than 1 suggest that while there's a strong correlation between the instruments, the GEMS operational product increases more than Pandora value for each NO_2 increase.

(b) GEMS IUP vs. Pandora: Similarly, a high R-value (0.96) with a slope greater (1.54) than 1 indicates a strong correlation but with GEMS IUP increasing more than Pandora for the same NO_2 increase.

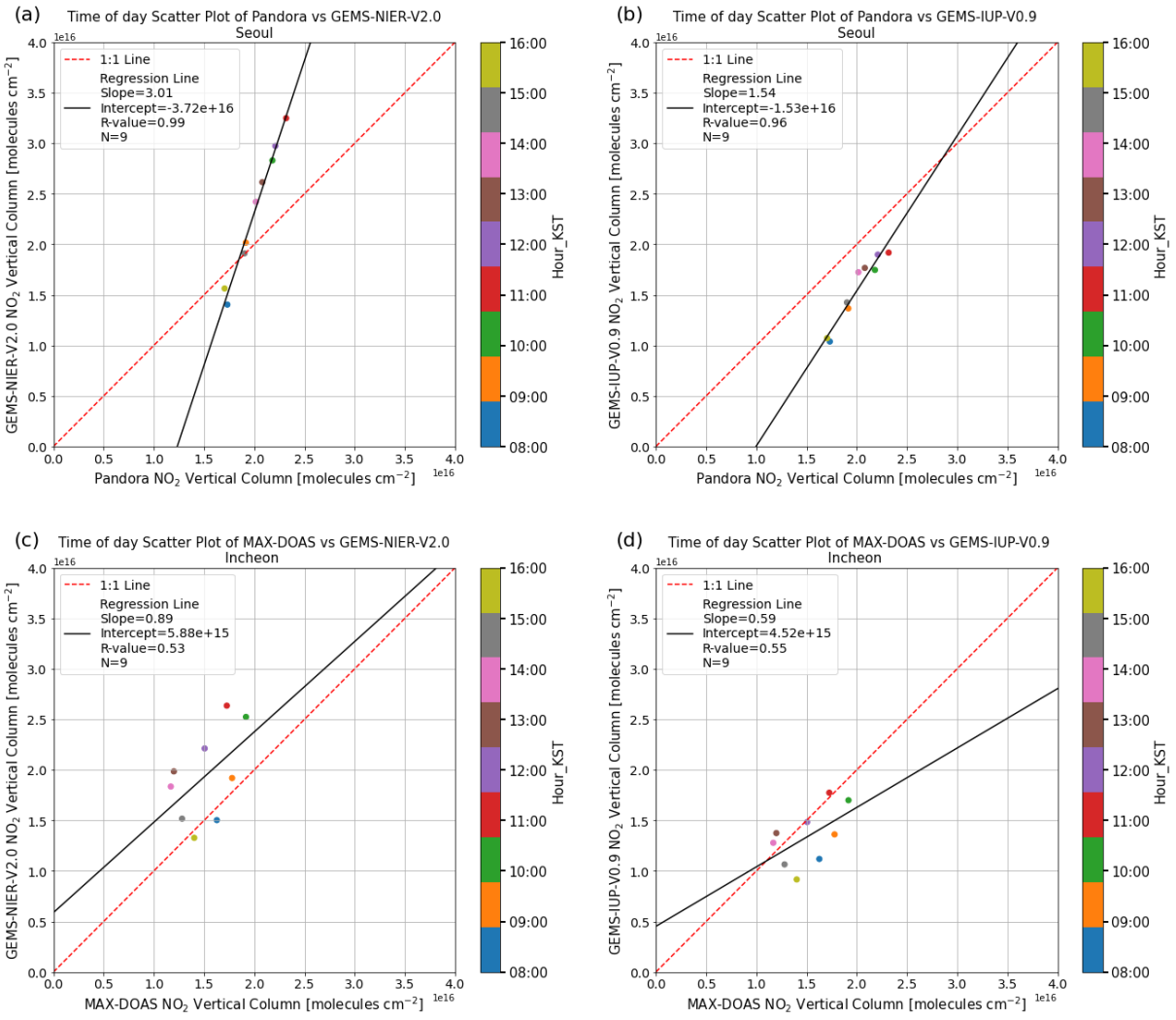

Figure 6.3.1. Scatter plot of time of the day mean tropospheric NO_2 vertical column (10^{16} molecules cm^{-2}). In this figure, hourly values were grouped and averaged over all the days of measurement then plotted from 08:00 to 16:00 local time (GEMS values only within this timeframe as seen in figure 5.2.1 to explain why there are 9 data points) in this case. The x and y axis labels remains the same as figure 6.2.1

Comparisons results in Incheon (c and d)

(c) GEMS operational product vs. MAX-DOAS: A moderate R-value (0.53) and a slope (0.89) less than 1 suggest a weaker correlation, with

GEMS operational product showing less increase compared to MAX-DOAS for the same NO_2 value increase.

(d) GEMS-IUP-V0.9 vs. MAX-DOAS: A moderate R-value (0.55) and a slope (0.59), similar to (c) also suggest a weaker correlation and less increase for GEMS IUP compared to MAX-DOAS.Therefore, the conclusion is that the operational product tends to strongly overestimate higher values and underestimate lower values. In contrast, the GEMS IUP product consistently underestimates observation values, displaying a similar pattern for both low and high values. However, the underestimation by the GEMS IUP product in Incheon is smaller compared to the observation in Seoul and the overestimation by the GEMS operational product in Incheon is smaller compared to the observation in Seoul. It's important to note that these observations are made under the condition of averaging over the full time of day. The discussion primarily focuses on the behaviour as a function of time of the day, as seasonal effects and variations across days of the week are not considered due to averaging over all seasons and days.

The difference between the two sites probably arises from the Pandora instrument being located in a central location within a highly polluted area, presenting a relatively homogeneous environment for measurements. In contrast, the MAX-DOAS instrument in Incheon is situated at the edge of the polluted zone, resulting in measurements showing greater heterogeneity. This spatial variation leads to significant biases between ground-level observations and satellite data. Seoul's large size and pollution levels result in consistent values within a 15km radius, both north and south. Incheon's location on the edge of the polluted area yields distinct variability of values within 15km radius affecting the agreement between satellite and ground-based measurements. The poorer correlation observed in Incheon can be attributed to this inherent inhomogeneity in the measurement environment.

6.4.1 Seasonal variation scatter plot of Ground-based and satellite observation

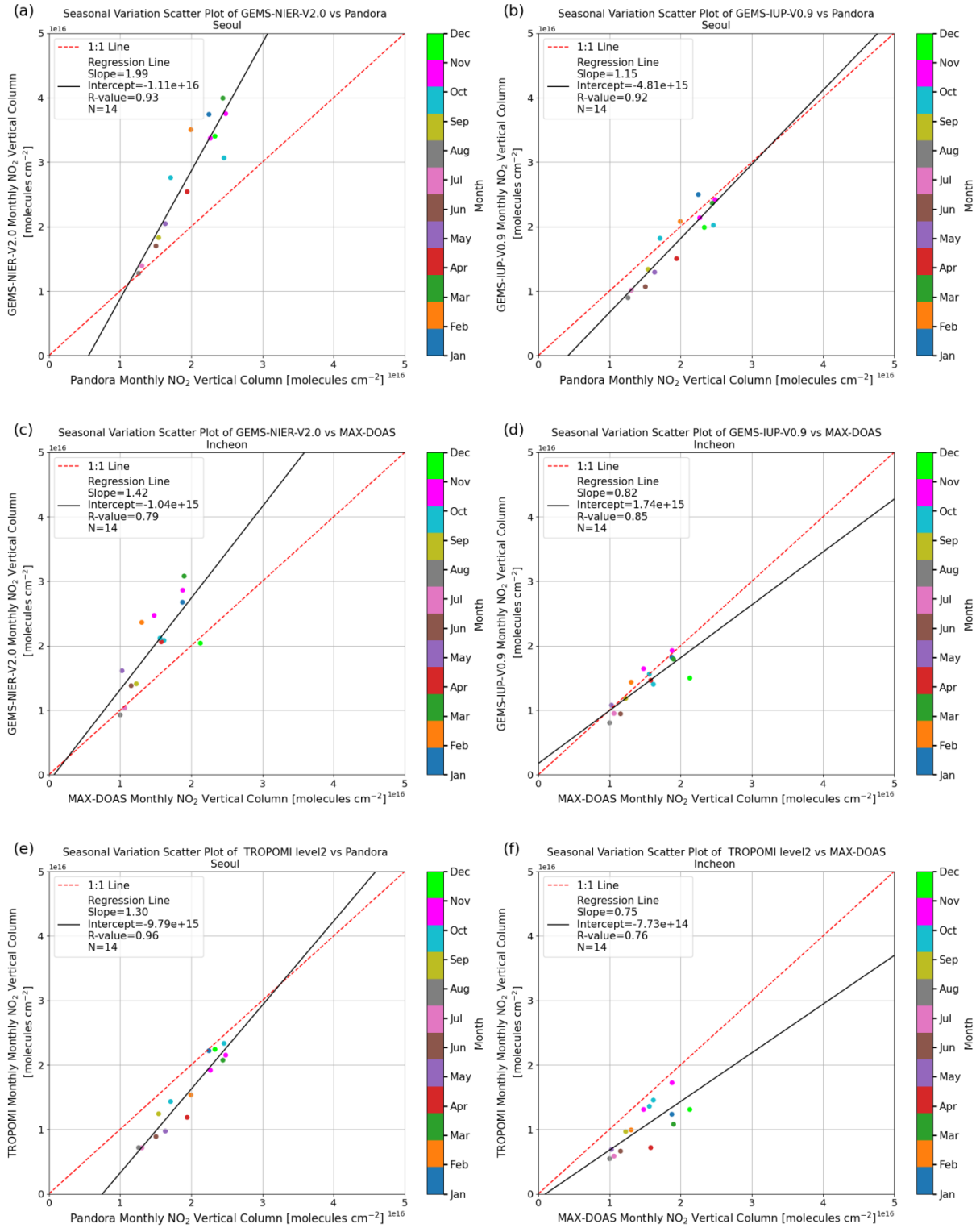

Figure 6.4.1. Scatter plot of average monthly tropospheric NO_2 vertical column (10^{16} molecules cm^{-2}). In this figure, monthly values are grouped and averaged then plotted in this case. The x and y axis labels remains the

same as figure 6.2.1 but with addition of (e) TROPOMI against Pandora in Seoul, and (d) TROPOMI against MAX-DOAS in Incheon.

Figure 6.4.1 shows scatter plots of average monthly tropospheric NO_2 vertical column for (GEMS operational, GEMS IUP and TROPOMI) product vs. Pandora and MAX-DOAS comparisons in Seoul and Incheon respectively.The result of figure 6.4.1 shows that, TROPOMI tends to measure lower values, resulting in an underestimation of NO_2 observations in both Seoul and Incheon. However, the GEMS operational product tends to overestimate the seasonal variation of NO_2. While the GEMS operational product overestimates NO_2 measurements, the GEMS IUP product underestimates NO_2 observations. When considering seasonality, it becomes clear that the GEMS IUP product outperforms the operational product in measuring the seasonal NO_2 variations.These observations align with the diurnal variation findings, indicating that the GEMS operational product tends to be too high, while the GEMS IUP product tends to be too low. Specifically in Incheon, the slope appears to be better aligned with the GEMS IUP product than with the GEMS operational product. When assessing the absolute differences between the products, it becomes evident that the GEMS IUP product exhibits smaller differences.

6.5.1 Comparison with previous studies

Similar to this study, Irie et al., (2008) found biases of have a positive bias of $1.6x10^{15}$ molecules cm^{-2} in satellite NO_2 data (OMI), although their study identified a consistent positive bias, while the current study found both overestimation and underestimation in GEMS products compared to ground measurements. Also, Kim et al. (2023), conducted validation in Seosan, South Korea, using GEMS Level 2 NO_2 vertical column and found correlation coefficients between GEMS and Pandora NO_2 data ranging from 0.35 to 0.48 without cloud condition corrections and 0.62 to 0.78 with corrections for less cloudy conditions. This study's findings show a similar trend with moderate to strong positive correlations observed between GEMS products and ground-based measurements, underscoring the ability of GEMS in NO_2 measurement, particularly in less cloudy conditions.. Stavrakou et al., (2020) focused on weekly NO_2 variations using OMI and TROPOMI data. Their study found that the OMI Saturday and Sunday percentage reduction of NO_2 for Seoul to be 13%, and 11%, and for Busan, 7% and 20% respectively.. They found that the TROPOMI reduction in Seoul were 13% and 11% , and for Busan, 7% , and 20% respectively. This study found that the GEMS and the TROPOMI Saturday and Sunday NO_2 reduction in Seoul to be 20% and 40%.

Chapter 7

Summary and Conclusions

Summary and key study findings

The study aimed to validate GEMS tropospheric NO_2 observation products by comparing them with results from ground-based MAX-DOAS and Pandora instruments, as well as the TROPOMI. The study utilized several datasets for a comparative analysis which includes the GEMS operational and IUP products, the TROPOMI product, ground-based measurements from the MAX-DOAS instrument at the National Institute of Environmental Research (NIER) headquarters in Incheon and also ground-based measurements from the Pandora instrument at Yonsei University, Seoul. The study evaluated various aspects of NO_2, such as: Hourly, diurnal, weekly, and seasonal variations in tropospheric NO_2 vertical columns, correlation between satellite products and ground-based observations. Then Measurement biases and accuracies of satellite observations compared to ground-based measurements.

The study conducted a detailed correlation and bias analysis, revealing strong correlations between GEMS products and ground-based measurements. The R-values indicated moderate to strong positive agreement, with the GEMS operational product versus Pandora showing 0.74, GEMS IUP versus Pandora at 0.84, GEMS operational product versus MAX-DOAS at 0.71, and GEMS IUP versus MAX-DOAS at 0.82. However, biases were identified, with the GEMS operational product tending to overestimate and the GEMS IUP product underestimating NO_2 levels in comparison to Pandora in Seoul and MAX-DOAS in Incheon.

In terms of Seasonal Variations, the study observed higher NO_2 levels during the colder months, from late October to early March, which were attributed to increased emissions from heating and slower atmospheric chemical reactions. However, during the summer months, from May to early September, lower NO_2 levels were observed, this is likely due to increased photolysis rates and heavy rainfall leading to NO_2 removal through wet deposition.

The analysis of Hourly Variations showed that in Seoul, peak NO_2 levels occurred between 10:00 and 12:00, with values around 2.32×10^{16} molecules cm^{-2}, as per Pandora measurements and 3.20×10^{16} molecules cm^{-2} as per the GEMS operational product. In Incheon, a distinct double-peak pattern was observed with MAX-DOAS measurements, peaking around 11:00 and 16:00. There was a better agreement between MAX-DOAS and GEMS IUP vertical

columns compared to the GEMS operational product data. Additionally, TROPOMI measurements showed lower values, likely due to their midday timing, in contrast to GEMS, which measures throughout the day.

In conclusion, the study successfully validated the GEMS NO_2 observation products, underscoring their ability in measuring tropospheric NO_2 vertical columns. These findings emphasize the importance of integrating satellite and ground-based measurements for comprehensive air quality monitoring. Despite strong correlations, the presence of biases in GEMS products necessitates on-going validation. The findings of this study have shown significant diurnal and seasonal variations in NO_2 levels, influenced by various factors including heating emissions, photolysis rates, and anthropogenic activities, is crucial for air quality management and public health policy-making, especially in regions like Seoul and Incheon where NO_2 pollution is a significant concern.

Outlook

As we have seen from the biases by the GEMS operational product and GEMS IUP product, with the bias in GEMS IUP lower. Therefore, new algorithms that can minimize the differences between satellite and ground-based measurements should be developed and implemented. Secondly, that the IUP product should in the future, include cloud and aerosol corrections as they are still missing. In addition, i recommend that the period of data collection be extended to include multiple years for assessing long-term variations.

Acknowledgments

The GEMS operational NO_2 data sets as well as the GEMS lv1 data used in this study were provided by NIER. TROPOMI lv2 data were provided by Copernicus. Pandora measurements in Seoul were provided by the PANDONIA web page. Financial support by NIER for ground-based measurements during the GMAP and SIJAQ is gratefully acknowledged.

References

Bae, Hyun-Joo, Jung Eun Kang, and Yu-Ra Lim. 'Assessing the Health Vulnerability Caused by Climate and Air Pollution in Korea Using the Fuzzy TOPSIS'. *Sustainability* 11, no. 10 (21 May 2019): 2894. https://doi.org/10.3390/su11102894

Bae, Kangho, Chang-Keun Song, Andreas Richter, Thomas Wagner, Michel Van Roozendael, Kezia Lange, Tim Boesch, et al. 'Preliminary Results of the GMAP/SIJAQ Campaign: Remote Sensing Measurements of Air Pollution over Korea'. Other. oral, 15 May 2023. https://doi.org/10.5194/egusphere-egu23-4636.

Beirle, Steffen, Christoph Hörmann, Patrick Jöckel, Song Liu, Marloes Penning De Vries, Andrea Pozzer, Holger Sihler, Pieter Valks, and Thomas Wagner. 'The STRatospheric Estimation Algorithm from Mainz (STREAM): Estimating Stratospheric NO2 from Nadir-Viewing Satellites by Weighted Convolution'. *Atmospheric Measurement Techniques* 9, no. 7 (4 July 2016): 2753–79. https://doi.org/10.5194/amt-9-2753-2016.

Boersma, K. Folkert, Daniel J. Jacob, Henk J. Eskes, Robert W. Pinder, Jun Wang, and Ronald J. Van Der A. 'Intercomparison of SCIAMACHY and OMI Tropospheric NO_2 Columns: Observing the Diurnal Evolution of Chemistry and Emissions from Space'. *Journal of Geophysical Research: Atmospheres* 113, no. D16 (27 August 2008): 2007JD008816. https://doi.org/10.1029/2007JD008816.

Bovensmann, H., J. P. Burrows, M. Buchwitz, J. Frerick, S. Noël, V. V. Rozanov, K. V. Chance, and A. P. H. Goede. 'SCIAMACHY: Mission Objectives and Measurement Modes'. *Journal of the Atmospheric Sciences* 56, no. 2 (January 1999): 127–50. https://doi.org/10.1175/1520-0469(1999)056<0127:SMOAMM>2.0.CO;2.

Bucsela, E. J., N. A. Krotkov, E. A. Celarier, L. N. Lamsal, W. H. Swartz, P. K. Bhartia, K. F. Boersma, J. P. Veefkind, J. F. Gleason, and K. E. Pickering. 'A New Stratospheric and Tropospheric NO_2 Retrieval Algorithm for Nadir-Viewing Satellite Instruments: Applications to OMI'. *Atmospheric Measurement Techniques* 6, no. 10 (15 October 2013): 2607–26. https://doi.org/10.5194/amt-6-2607-2013.

Burrows, J.P., E. Hölzle, A.P.H. Goede, H. Visser, and W. Fricke. 'SCIAMACHY—Scanning Imaging Absorption Spectrometer for Atmospheric Chartography'. *Acta Astronautica* 35, no. 7 (April 1995): 445–51. https://doi.org/10.1016/0094-5765(94)00278-T.

Burrows, John P., Mark Weber, Michael Buchwitz, Vladimir Rozanov, Annette Ladstätter-Weißenmayer, Andreas Richter, Rüdiger DeBeek, et al. 'The Global Ozone Monitoring Experiment (GOME): Mission Concept and First Scientific Results'. *Journal of the Atmospheric Sciences* 56, no. 2 (January 1999): 151–75. https://doi.org/10.1175/1520-0469(1999)056<0151:TGOMEG>2.0.CO;2.

Chauhan, Aj, Hazel M Inskip, Catherine H Linaker, Sandra Smith, Jacqueline Schreiber, Sebastian L Johnston, and Stephen T Holgate. 'Personal Exposure to Nitrogen Dioxide (NO_2) and the Severity of Virus-Induced Asthma in Children'. *The Lancet* 361, no. 9373 (June 2003): 1939–44. https://doi.org/10.1016/S0140-6736(03)13582-9.

De Smedt, Isabelle, Gaia Pinardi, Corinne Vigouroux, Steven Compernolle, Alkis Bais, Nuria Benavent, Folkert Boersma, et al. 'Comparative Assessment of TROPOMI and OMI Formaldehyde Observations and Validation against MAX-DOAS Network Column Measurements'. *Atmospheric Chemistry and Physics* 21, no. 16 (23 August 2021): 12561–93. https://doi.org/10.5194/acp-21-12561-2021.

Dong, Yun, Elena Spinei, and Anuj Karpatne. 'A Feasibility Study to Use Machine Learning as an Inversion Algorithm for Aerosol Profile and Property Retrieval from Multi-Axis Differential Absorption Spectroscopy Measurements'. *Atmospheric Measurement Techniques* 13, no. 10 (16 October 2020): 5537–50. https://doi.org/10.5194/amt-13-5537-2020.

Europe, Spectroscopy. 'Differential Optical Absorption Spectroscopy as a Tool to Measure Pollution from Space'. Text. Accessed 1 December 2023. https://www.spectroscopyeurope.com/article/differential-optical-absorption-spectroscopy-tool-measure-pollution-space.

Finlayson-Pitts, Barbara J., and James N. Pitts. 'CHAPTER 3 - Spectroscopy and Photochemistry: Fundamentals'. In *Chemistry of the Upper and Lower Atmosphere*, edited by Barbara J. Finlayson-Pitts and James N. Pitts, 43–85. San Diego: Academic Press, 2000. https://doi.org/10.1016/B978-012257060-5/50005-8.

Finlayson-Pitts, Barbara J., and James N. Pitts. 'CHAPTER 4 - Photochemistry of Important Atmospheric Species'. In *Chemistry of the Upper and Lower Atmosphere*, edited by Barbara J. Finlayson-Pitts and James N. Pitts, 86–129. San Diego: Academic Press, 2000. https://doi.org/10.1016/B978-012257060-5/50006-X.

Herman, Jay, Alexander Cede, Elena Spinei, George Mount, Maria Tzortziou, and Nader Abuhassan. 'NO_2 Column Amounts from Ground-based Pandora and MFDOAS Spectrometers Using the Direct-sun DOAS Technique: Intercomparisons and Application to OMI Validation'. *Journal of Geophysical Research: Atmospheres* 114, no. D13 (16 July 2009): 2009JD011848. https://doi.org/10.1029/2009JD011848.

Hönninger, G., C. Von Friedeburg, and U. Platt. 'Multi Axis Differential Optical Absorption Spectroscopy (MAX-DOAS)'. *Atmospheric Chemistry and Physics* 4, no. 1 (9 February 2004): 231–54. https://doi.org/10.5194/acp-4-231-2004.

Huijnen, V., J. Williams, M. van Weele, T. van Noije, M. Krol, F. Dentener, A. Segers, et al. 'The Global Chemistry Transport Model TM5: Description and Evaluation of the Tropospheric

Chemistry Version 3.0'. *Geoscientific Model Development* 3, no. 2 (6 October 2010): 445–73. https://doi.org/10.5194/gmd-3-445-2010.

Irie, H., Y. Kanaya, H. Akimoto, H. Tanimoto, Z. Wang, J. F. Gleason, and E. J. Bucsela. 'Validation of OMI Tropospheric NO_2 Column Data Using MAX-DOAS Measurements Deep inside the North China Plain in June 2006: Mount Tai Experiment 2006'. *Atmospheric Chemistry and Physics* 8, no. 22 (17 November 2008): 6577–86. https://doi.org/10.5194/acp-8-6577-2008.

Irie, H., H. Takashima, Y. Kanaya, K. F. Boersma, L. Gast, F. Wittrock, D. Brunner, Y. Zhou, and M. Van Roozendael. 'Eight-Component Retrievals from Ground-Based MAX-DOAS Observations'. *Atmospheric Measurement Techniques* 4, no. 6 (9 June 2011): 1027–44. https://doi.org/10.5194/amt-4-1027-2011.

Judd, Laura M., Jassim A. Al-Saadi, Lukas C. Valin, R. Bradley Pierce, Kai Yang, Scott J. Janz, Matthew G. Kowalewski, James J. Szykman, Martin Tiefengraber, and Moritz Mueller. 'The Dawn of Geostationary Air Quality Monitoring: Case Studies From Seoul and Los Angeles'. *Frontiers in Environmental Science* 6 (15 August 2018): 85. https://doi.org/10.3389/fenvs.2018.00085.

Kim, Jhoon, Ukkyo Jeong, Myoung-Hwan Ahn, Jae H. Kim, Rokjin J. Park, Hanlim Lee, Chul Han Song, et al. 'New Era of Air Quality Monitoring from Space: Geostationary Environment Monitoring Spectrometer (GEMS)'. *Bulletin of the American Meteorological Society* 101, no. 1 (January 2020): E1–22. https://doi.org/10.1175/BAMS-D-18-0013.1.

Kim, Moon Joon. 'The Effects of Transboundary Air Pollution from China on Ambient Air Quality in South Korea'. *Heliyon* 5, no. 12 (December 2019): e02953. https://doi.org/10.1016/j.heliyon.2019.e02953.

Kim, P. S., D. J. Jacob, J. A. Fisher, K. Travis, K. Yu, L. Zhu, R. M. Yantosca, et al. 'Sources, Seasonality, and Trends of Southeast US Aerosol: An Integrated Analysis of Surface, Aircraft, and Satellite Observations with the GEOS-Chem Chemical Transport Model'. *Atmospheric Chemistry and Physics* 15, no. 18 (23 September 2015): 10411–33. https://doi.org/10.5194/acp-15-10411-2015.

Kim, Serin, Daewon Kim, Hyunkee Hong, Lim-Seok Chang, Hanlim Lee, Deok-Rae Kim, Donghee Kim, et al. 'First-Time Comparison between NO_2 Vertical Columns from Geostationary Environmental Monitoring Spectrometer (GEMS) and Pandora Measurements'. *Atmospheric Measurement Techniques* 16, no. 16 (30 August 2023): 3959–72. https://doi.org/10.5194/amt-16-3959-2023.

Kim, Yong Pyo, and Gangwoong Lee. 'Trend of Air Quality in Seoul: Policy and Science'. *Aerosol and Air Quality Research* 18, no. 9 (2018): 2141–56. https://doi.org/10.4209/aaqr.2018.03.0081.

Lee, Kyung-Shin, Youn-Hee Lim, Yoon-Jung Choi, Soontae Kim, Hyun Joo Bae, Changwoo Han, Young Ah Lee, and Yun-Chul Hong. 'Prenatal Exposure to Traffic-Related Air Pollution and Risk of Congenital Diseases in South Korea'. *Environmental Research* 191 (December 2020): 110060. https://doi.org/10.1016/j.envres.2020.110060.

Lee, Won-Jin, Dongwon Lee, Jhoon Kim, Myoung Hwan Ahn, Jae Kim, Rokjin Park, Hanlim Lee, et al. 'Geostationary Environmental Monitoring Spectrometer (GEMS) Status, Preliminary Results and Validation Campaign' 2021 (1 December 2021): A11A-01. https://ui.adsabs.harvard.edu/abs/2021AGUFM.A11A..01L.

Leem, Jong Han, Soon Tae Kim, and Hwan Cheol Kim. 'Public-Health Impact of Outdoor Air Pollution for 2nd Air Pollution Management Policy in Seoul Metropolitan Area, Korea'. *Annals of Occupational and Environmental Medicine* 27, no. 1 (December 2015): 7. https://doi.org/10.1186/s40557-015-0058-z.

Leue, C., M. Wenig, T. Wagner, Oliver Klimm, U. Platt, and B. Jähne. 'Quantitative Analysis of NO_x Emissions from Global Ozone Monitoring Experiment Satellite Image Sequences'. *Journal of Geophysical Research: Atmospheres* 106, no. D6 (27 March 2001): 5493–5505. https://doi.org/10.1029/2000JD900572.

Lonsdale, Chantelle R., and Kang Sun. 'Nitrogen Oxides Emissions from Selected Cities in North America, Europe, and East Asia Observed by the TROPOspheric Monitoring Instrument (TROPOMI) before and after the COVID-19 Pandemic'. *Atmospheric Chemistry and Physics* 23, no. 15 (8 August 2023): 8727–48. https://doi.org/10.5194/acp-23-8727-2023.

Ma, J. Z., S. Beirle, J. L. Jin, R. Shaiganfar, P. Yan, and T. Wagner. 'Tropospheric NO_2 Vertical Column Densities over Beijing: Results of the First Three Years of Ground-Based MAX-DOAS Measurements (2008–2011) and Satellite Validation'. *Atmospheric Chemistry and Physics* 13, no. 3 (7 February 2013): 1547–67. https://doi.org/10.5194/acp-13-1547-2013.

Mayer, Helmut. 'Air Pollution in Cities'. *Atmospheric Environment* 33, no. 24–25 (October 1999): 4029–37. https://doi.org/10.1016/S1352-2310(99)00144-2.

Meng, Xia, Cong Liu, Renjie Chen, Francesco Sera, Ana Maria Vicedo-Cabrera, Ai Milojevic, Yuming Guo, et al. 'Short Term Associations of Ambient Nitrogen Dioxide with Daily Total, Cardiovascular, and Respiratory Mortality: Multilocation Analysis in 398 Cities'. *BMJ*, 24 March 2021, n534. https://doi.org/10.1136/bmj.n534.

Mie, Gustav. 'Beiträge Zur Optik Trüber Medien, Speziell Kolloidaler Metallösungen'. *Annalen Der Physik* 330, no. 3 (January 1908): 377–445. https://doi.org/10.1002/andp.19083300302.

Ngarambe, Jack, Soo Jeong Joen, Choong-Hee Han, and Geun Young Yun. 'Exploring the Relationship between Particulate Matter, CO, SO_2, NO_2, O_3 and Urban Heat Island in Seoul, Korea'. *Journal of Hazardous Materials* 403 (5 February 2021): 123615. https://doi.org/10.1016/j.jhazmat.2020.123615.

Park, Hyeon-Ju, Jin-Soo Park, Sang-Woo Kim, Heesung Chong, Hana Lee, Hyunjae Kim, Joon-Young Ahn, Dai-Gon Kim, Jhoon Kim, and Sang Seo Park. 'Retrieval of NO_2 Column

Amounts from Ground-Based Hyperspectral Imaging Sensor Measurements'. *Remote Sensing* 11, no. 24 (13 December 2019): 3005. https://doi.org/10.3390/rs11243005.

Park, Jin-Ok, Sanghoo Yoon, Myung Hwan Na, and Ho-Chun Song. 'The Effects of Air Pollution on Mortality in South Korea'. *Procedia Environmental Sciences* 26 (2015): 62–65. https://doi.org/10.1016/j.proenv.2015.05.025.

Park, Junsung, Hanlim Lee, Hyunkee Hong, Jiwon Yang, Michel Van Roozendael, Siwan Kim, Jhoon Kim, et al. 'First Results of Diurnal NO_2 Column Variation over Asia from the Geostationary Environment Monitoring Spectrometer (GEMS) '; Other. display, 27 March 2022. https://doi.org/10.5194/egusphere-egu22-3280.

Pinardi, Gaia, Michel Van Roozendael, François Hendrick, Nicolas Theys, Nader Abuhassan, Alkiviadis Bais, Folkert Boersma, et al. 'Validation of Tropospheric NO_2 Column Measurements of GOME-2A and OMI Using MAX-DOAS and Direct Sun Network Observations'. Preprint. Gases/Remote Sensing/Validation and Intercomparisons, 30 March 2020. https://doi.org/10.5194/amt-2020-76.

Piters, A. J. M., K. Bramstedt, J.-C. Lambert, and B. Kirchhoff. 'Overview of SCIAMACHY Validation: 2002–2004'. *Atmospheric Chemistry and Physics* 6, no. 1 (25 January 2006): 127–48. https://doi.org/10.5194/acp-6-127-2006.

Platt, Ulrich, and Jochen Stutz. 'Differential Absorption Spectroscopy'. In *Differential Optical Absorption Spectroscopy: Principles and Applications*, edited by Ulrich Platt and Jochen Stutz, 135–74. Physics of Earth and Space Environments. Berlin, Heidelberg: Springer, 2008. https://doi.org/10.1007/978-3-540-75776-4_6.

Richter, A., and J.P. Burrows. 'Tropospheric NO2 from GOME Measurements'. *Advances in Space Research* 29, no. 11 (June 2002): 1673–83. https://doi.org/10.1016/S0273-1177(02)00100-X.

Rozanov, A., H. Bovensmann, A. Bracher, S. Hrechanyy, V. Rozanov, M. Sinnhuber, F. Stroh, and J.P. Burrows. 'NO2 and BrO Vertical Profile Retrieval from SCIAMACHY Limb Measurements: Sensitivity Studies'. *Advances in Space Research* 36, no. 5 (2005): 846–54. https://doi.org/10.1016/j.asr.2005.03.013.

Russell, A. R., L. C. Valin, and R. C. Cohen. 'Trends in OMI NO_2 Observations over the United States: Effects of Emission Control Technology and the Economic Recession'. *Atmospheric Chemistry and Physics* 12, no. 24 (21 December 2012): 12197–209. https://doi.org/10.5194/acp-12-12197-2012.

Seo, Seunghwan, Si-Wan Kim, Kyoung-Min Kim, Lok N Lamsal, and Hyungah Jin. 'Reductions in NO_2 Concentrations in Seoul, South Korea Detected from Space and Ground-Based Monitors Prior to and during the COVID-19 Pandemic'. *Environmental Research Communications* 3, no. 5 (1 May 2021): 051005. https://doi.org/10.1088/2515-7620/abed92.

Stavrakou, T., J.-F. Müller, M. Bauwens, K. F. Boersma, and J. Van Geffen. 'Satellite Evidence for Changes in the NO_2 Weekly Cycle over Large Cities'. *Scientific Reports* 10, no. 1 (22 June 2020): 10066. https://doi.org/10.1038/s41598-020-66891-0.

Strutt, J.W. 'XV. On the Light from the Sky, Its Polarization and Colour'. *The London, Edinburgh, and Dublin Philosophical Magazine and Journal of Science* 41, no. 271 (February 1871): 107–20. https://doi.org/10.1080/14786447108640452.

Vandaele, A. C., C. Fayt, F. Hendrick, C. Hermans, F. Humbled, M. Van Roozendael, M. Gil, et al. 'An Intercomparison Campaign of Ground-based UV-visible Measurements of NO $_2$, BrO, and OClO Slant Columns: Methods of Analysis and Results for NO_2'. *Journal of Geophysical Research: Atmospheres* 110, no. D8 (27 April 2005): 2004JD005423. https://doi.org/10.1029/2004JD005423.

Veefkind, Pepijn, Ilse Aben, Angelika Dehn, Quintus Kleipool, Diego Loyola, Andreas Richter, Michel van Roozendael, et al. 'Sentinel 5 Precursor: Status of TROPOMI and the Operational Data Products'. Copernicus Meetings, 9 March 2020. https://doi.org/10.5194/egusphere-egu2020-6895.

Verhoelst, Tijl, Steven Compernolle, Gaia Pinardi, Jean-Christopher Lambert, Henk J. Eskes, Kai-Uwe Eichmann, Ann Mari Fjæraa, et al. 'Ground-Based Validation of the Copernicus Sentinel-5P TROPOMI NO_2 Measurements with the NDACC ZSL-DOAS, MAX-DOAS and Pandonia Global Networks'. *Atmospheric Measurement Techniques* 14, no. 1 (22 January 2021): 481–510. https://doi.org/10.5194/amt-14-481-2021.

Williams, Jason E., K. Folkert Boersma, Phillipe Le Sager, and Willem W. Verstraeten. 'The High-Resolution Version of TM5-MP for Optimized Satellite Retrievals: Description and Validation'. *Geoscientific Model Development* 10, no. 2 (15 February 2017): 721–50. https://doi.org/10.5194/gmd-10-721-2017.

Zhou, B., S. N. Yang, S. S. Wang, and T. Wagner. 'Determination of an Effective Trace Gas Mixing Height by Differential Optical Absorption Spectroscopy (DOAS)'. Preprint. Gases/Remote Sensing/Data Processing and Information Retrieval, 20 July 2009. https://doi.org/10.5194/amtd-2-1663-2009.

Sentinel Online. 'DOAS Method - Level-2 Processing - Sentinel-5P Technical Guide - Sentinel Online'. Accessed 1 December 2023. https://copernicus.eu/technical-guides/sentinel-5p/level-2/doas-method.

Sentinel Online. 'DOAS Method - Level-2 Processing - Sentinel-5P Technical Guide - Sentinel Online'. Accessed 1 December 2023. https://copernicus.eu/technical-guides/sentinel-5p/level-2/doas-method.

Institute of Environmental Physics (IUP), University of Bremen. Stratospheric Observations (zenith-sky DOAS). Available online at: https://www.iup.uni-bremen.de/doas/maxdoas_instrument.htm (last access: 11 November 2023).

New NASA Satellite Maps Show Human Fingerprint on Global Air Quality - NASA'. Accessed 1 December 2023. https://www.nasa.gov/news-release/new-nasa-satellite-maps-show-human-fingerprint-on-global-air-quality/.

University of Bremen Practical Environmental Measurement Techniques Institute of Environmental Physics (IUP), Supervised by Midhun George and M. D. Andrés Hernández. Rayleigh scattering of standard molecules using Cavity Ring-Down Spectroscopy Last revised on 01.03.2019. 2019. https://www.msc-ep.uni-bremen.de/services/lectures/practicals/pr_crds_19.pdf

'PORT Of ULSAN'. Accessed 1 December 2023. https://ulsan.mof.go.kr/en/page.do?menuIdx=1523.

'SIJAQ'. Accessed 1 December 2023. https://www.sijaq.org/.

'SIJAQ 2022'. Accessed 1 December 2023. https://sijaq2.sijaq.org/.

'Incheon'. In *Wikipedia*, 15 November 2023. https://en.wikipedia.org/w/index.php?title=Incheon&oldid=1185284469.

'Seoul'. In *Wikipedia*, 29 November 2023. https://en.wikipedia.org/w/index.php?title=Seoul&oldid=1187437054.